Bulletin of Volcanology

Estimating eruptive parameters and related uncertainties for pyroclastic density currents deposits: worked examples from Somma-Vesuvius (Italy)

--Manuscript Draft--

Manuscript Number:	BUVO-D-20-00004R2
Full Title:	Estimating eruptive parameters and related uncertainties for pyroclastic density currents deposits: worked examples from Somma-Vesuvius (Italy)
Article Type:	Research Article
Corresponding Author:	Alessandro Tadini Universite Clermont Auvergne Aubière, Auvergne-Rhone-Alps FRANCE
Corresponding Author Secondary Information:	
Order of Authors:	Raffaello Cioni, Ph.D
	Alessandro Tadini, Ph.D.
	Lucia Gurioli, Ph.D.
	Antonella Bertagnini, Ph.D.
	Maurizio Mulas, Ph.D.
	Andrea Bevilacqua, Ph.D.
	Augusto Neri, Ph.D.
Funding Information:	Dipartimento della Protezione Civile, Presidenza del Consiglio dei Ministri (Project V1) — Dr. Augusto Neri
Abstract:	The quantification of the maximum runout, invaded area, volume and total grain-size distribution (TGSD) of pyroclastic density currents (PDC) is a critically important task because such parameters represent the needed input quantities for physical modeling and for hazard assessment of PDCs. In this work, new and well-established methods for the quantification of these parameters are applied to a large stratigraphic dataset of three PDC units from two eruptions of Somma-Vesuvius (the AD 79 Pompeii and the AD 472 Pollena eruptions), representative of a large spectrum of transport and depositional processes. Maximum runout and invaded area are defined on the basis of the available volcanological and topographical constraints. The related uncertainties are evaluated with an expert judgement procedure, which considered the different sectors of the volcano separately. Quite large uncertainty estimates of dispersal area (20-40%) may have important implications in terms of hazard assessment. The testing of different methods for estimating the volume (and mass) of a PDC deposit suggests that integration, over the invaded area, of thickness (and deposit density) data using the triangulated irregular network method can minimize and localize data extrapolation. Such calculations, however, bear an intrinsic additional uncertainty (at least 10% of the total PDC deposit) related to loss or new formation of fine material during transport (at least 10% of the total PDC deposit). Different interpolation methods for TGSD produce multimodal distributions, likely reflecting the different response of each grain size class to transport and deposition processes. These data, when integrated with information on the related co-ignimbrite deposits, can give a more accurate picture of the pyroclastic mixture feeding the current.
Response to Reviewers:	Dear Associate Editor, we have addressed all the requests for the revision, which are detailed in the following letter and in the manuscript with tracked changes. Furthermore, we have embedded figure captions in each figure's file, and we have checked the formatting of the references and the bibliography. Please let us know if you need also the figures withouth the captions.

	Best Regards Alessandro Tadini (on behalf of all the other co-authors)
Author Comments:	Dear publication office, as I have written to Fran van wyk de vries today, I am not able to link my current BV account to my ORCID account due to a previous BV account of mine with another email (not active anymore) which is linked to my ORCID account. If it is possible to delete my old account and merge the information from the old account to my current account that would be great. If not, could you please delete the old account? Thanks a lot for your help Best Regards Alessandro Tadini

Estimating eruptive parameters and related uncertainties for pyroclastic density currents deposits: worked examples from Somma-Vesuvius (Italy)

Raffaello Cioni[1,2], Alessandro Tadini[1,3*†], Lucia Gurioli[4], Antonella Bertagnini[3], Maurizio Mulas[5], Andrea Bevilacqua[3], Augusto Neri[3]

[1]Dipartimento di Scienze della Terra, Università di Firenze, Via G. La Pira, 4 – 50121 Firenze, Italy.

[2]Consiglio Nazionale delle Ricerche, Ist. di Geoscienze e Georisorse, SS Firenze, Via G. La Pira, 4 - 50121 Firenze, Italy.

[3]Istituto Nazionale di Geofisica e Vulcanologia, Sezione di Pisa, Via Cesare Battisti, 53 – 56125 Pisa, Italy.

[4]Laboratoire Magmas et Volcans, Univeristé Clermont Auvergne, CNRS, IRD, OPGC, Campus Universitaire des Cézeaux 6 Avenue Blaise Pascal TSA 60026 – CS 60026 63178 Aubiere Cedex, France.

[5]Escuela Superior Politécnica del Litoral, ESPOL, Facultad de Ingeniería en Ciencias de la Tierra, Campus Gustavo Galindo Km 30.5 Vía Perimetral, P.O. Box 09-01-5863, Guayaquil, Ecuador.

*Corresponding author: Alessandro Tadini (Alessandro.TADINI@uca.fr)

[†]Current address: Laboratoire Magmas et Volcans, Univeristé Clermont Auvergne, CNRS, IRD, OPGC, Campus Universitaire des Cézeaux 6 Avenue Blaise Pascal TSA 60026 – CS 60026 63178 Aubiere Cedex, France

ORCID IDs

Raffaello Cioni : 0000-0002-2526-9095

Alessandro Tadini : 0000-0003-3603-0853

Lucia Gurioli : 0000-0002-5066-5153

Antonella Bertagnini : 0000-0003-4075-2242

Maurizio Mulas : 0000-0002-2089-3980

Andrea Bevilacqua : 0000-0002-0724-2593

Augusto Neri : 0000-0002-3536-3624

Acknowledgements

Marina Bisson is acknowledged for several useful discussions during the development of the manuscript, which greatly improved its quality. This paper was greatly improved by the detailed and insightful comments of Greg Valentine and of an anonymous reviewer. We also thank the editorial handling of Richard J. Brown.

Funding information

This work has been partially supported by the project V1 "Stima della pericolosità vulcanica in termini probabilistici" funded by Dipartimento della Protezione Civile (Italy). The manuscript does not necessarily represent official views and policies of the Dipartimento della Protezione Civile.

Availability of data and material

The Online Resources presented in this study could be found also in a repository in the Figshare community with the following DOI: 10.6084/m9.figshare.12506027.

Abstract

The quantification of the maximum runout, invaded area, volume and total grain-size distribution (TGSD) of pyroclastic density currents (PDC) is a critically important task because such parameters represent the needed input quantities for physical modeling and for hazard assessment of PDCs. In this work, new and well-established methods for the quantification of these parameters are applied to a large stratigraphic dataset of three PDC units from two eruptions of Somma-Vesuvius (the AD 79 Pompeii and the AD 472 Pollena eruptions), representative of a large spectrum of transport and depositional processes. Maximum runout and invaded area are defined on the basis of the available volcanological and topographical constraints. The related uncertainties are evaluated with an expert judgement procedure, which considered the different sectors of the volcano separately. Quite large uncertainty estimates of dispersal area (20-40%) may have important implications in terms of hazard assessment. The testing of different methods for estimating the volume (and mass) of a PDC deposit suggests that integration, over the invaded area, of thickness (and deposit density) data using the triangulated irregular network method can minimize and localize data extrapolation. Such calculations, however, bear an intrinsic additional uncertainty (at least 10% of the total PDC deposit) related to loss or new formation of fine material during transport (at least 10% of the total PDC deposit). Different interpolation methods for TGSD produce multimodal distributions, likely reflecting the different response of each grain size class to transport and deposition processes. These data, when integrated with information on the related co-ignimbrite deposits, can give a more accurate picture of the pyroclastic mixture feeding the current.

Keywords

Pyroclastic Density Currents; Somma-Vesuvius; maximum runout; volume; total grain size distribution; uncertainty quantification

1. Introduction

The starting point for the assessment of volcanic hazard is an accurate reconstruction of the eruptive history of a volcano, which in turn relies upon the availability of detailed field data that provide physical characterization of the possible outcomes of a future eruption (Neri et al. 2008). While methods for estimating eruption source parameters related to tephra fallout are clearly defined and numerical modeling has been generally developed based on these data (Biass et al. 2014), measurements on pyroclastic density current (PDC – called also pyroclastic currents) deposits have been used only recently to constrain the related numerical models (e.g., Esposti Ongaro et al. 2012, 2016; Spiller et al. 2014). Some of the most important parameters that need to be evaluated to **c**onstrain PDC-related hazards are: a) maximum runout distance, b) extent of invaded area, c) total volume and d) total grain size distribution (TGSD) of the flow mixture. In parallel, sedimentological investigations on the deposits aimed at defining the main transport and depositional processes of the parental current are fundamental for the definition of the assumptions that have to be made in the physical modeling, and hence of the models to be used (Patra et al. 2018, 2020). Despite several attempts to estimate these parameters for PDCs, the latter are known to be affected by several sources of epistemic uncertainty (see Bevilacqua et al. 2017; Rutarindwa et al. 2019). Presently the volcanological community lacks a standardized approach for estimating PDC-related parameters from their deposits. This is primarily due to the complexity of the depositional processes, which are strongly controlled by the interaction of the current with the underlying topography and by the mechanics of particle transport in the different regions of the current: such complexity prevents the description of the thickness or grain-size of PDC deposits simply as a function of the distance from the vent (Druitt 1998; Branney and Kokelaar 2002).

Here we quantify key parameters for a range of PDC deposits at Somma-Vesuvius volcano that can be used as input data for numerical simulations for volcanic hazard assessment, and to provide extensive uncertainty quantification. The different methodologies presented and discussed here provide a blueprint for the development of standard procedures for the assessment of these important parameters and the related uncertainty. We present new and revised data from PDC deposits from two different eruptions at Somma-Vesuvius (Fig. 1): i) the AD 79 Pompeii Plinian eruption and ii) the AD 472 Pollena sub-Plinian eruption. These PDC deposits resulted from different transport and deposition conditions, allowing us to test different methods of estimation over diverse natural conditions. Therefore, for each of the previously listed parameters, different methods were refined and used for their quantification, results obtained for the same parameter from different methods were compared and discussed, and an average value among the methods is provided for each parameter.

2. Types of pyroclastic density currents at Somma-Vesuvius

We consider two end-member types of PDCs, common during Plinian and sub-Plinian eruptions (Cioni et al. 2004; Cioni et al. 2008):

i) dilute PDCs, where turbulence is the main supporting mechanism (Branney and Kokelaar 2002). Deposits from this type of PDC are here represented by the EU3pf (Fig. 2a) and EU4b (Fig. 2b) PDC units from the AD 79 Pompeii eruption (Cioni et al. 2004; Gurioli et al. 2007). They are composed of tuff and fine lapilli tuff, and characterized by a progressive, although irregular, variation of grainsize, texture and thickness with distance from source and by the presence of traction structures such as planar and cross beds with internal coarse-tail grading.

ii) dense PDCs, where transport of particles is dominated by collisional momentum transfer between grains (Branney and Kokelaar 2002). Deposits of this type are represented by two PDC lobes (i.e. the "Cupa Olivella" and "Cupa Fontana") belonging to the F_g unit of the AD 472 Pollena eruption (Sulpizio et al. 2005; Sulpizio et al. 2007). They are characterized by massive deposits up to 12 meters thick that are mainly confined to deeper paleovalleys, and that exhibit no variation in grainsize with distance (Fig. 2c).

2.1 AD 79 deposits

Cioni et al. (1992) divided the AD 79 eruptive sequence into 8 main eruptive units (EU1-EU8) and some minor sub-units. Three main phases of the eruption (opening phase, Plinian phase and phreatomagmatic phase) were distinguished and PDC deposits are mainly related to the last two phases (Cioni et al. 1992).

The PDC deposits of the EU3pf unit (Fig. 2a) are considered to be derived from the final collapse of the Plinian column (Cioni et al. 2004). They are typically about one meter thick, are radially dispersed up to 10 km from vent, and have complex vertical and lateral facies variability (Gurioli 1999; Gurioli et al. 1999) that can be ascribed to local variation in turbulence and particle concentration and to the stratification of the current. Median clast size tends to diminish gradually from proximal to distal locations, and the coarsest deposits (generally present as tuff breccia lenses in the EU3pf sequence) are located within paleodepressions. Gurioli et al. (1999) noted that: i) in the southern part of the Somma-Vesuvius area (see Fig. 3) the relatively smooth paleo-topography exerted only localized control on the overall deposition of the PDC; ii) in the eastern sector of Somma-Vesuvius, where the current climbed over the remnants of the old Mount Somma scarp, the paleotopography induced a general increase of the current turbulence and velocity and more efficient air ingestion; iii) in the western sector of Somma-Vesuvius (Fig. 3), the presence of a breach in the caldera wall and a major break in slope in the area of Piano delle Ginestre (see Fig. 3), possibly increased deposition from the PDC, producing a large depositional fan with thicknesses up to several meters toward sea-facing sectors (e.g., in Ercolano, Fig. 1); iv) in the northern sector of Somma-Vesuvius (see Fig. 3), the deeply eroded paleotopography (with many valleys and steep slopes) favored the development within the whole current of a fast-moving, dense basal underflow confined in the main valleys, with a slower and more dilute portion travelling along morphological highs.

The AD 79 EU4 unit (Fig. 2b) resulted from a short-lived column that emplaced three distinct layers (Cioni et al. 1992): a thin, basal fallout layer ("EU4a", Fig. 2b); a PDC deposit which represents on average 60-90% of the total EU4 thickness, interpreted as the result of column collapse ("EU4b", Fig. 2b); a co-ignimbrite ash fall layers relating to EU4b ("EU4c", Fig. 2b). The runout of the EU4b PDC is one of the greatest observed for PDCs at Somma-Vesuvius (20 km; Gurioli et al. 2010) and it reached the area presently occupied by the town of Nocera Inferiore (Fig. 1). This unit has been extensively studied by Gurioli (1999) and Gurioli et al. (2005), who highlighted that: i) EU4b shows clear vertical grain size and textural variations, and varies from cross bedded, fine lapilli to coarse ash laminae at the base to a massive, fine ash-bearing, poorly sorted, matrix-supported bed at top; ii) the extended erosion of the pumice-bearing layer of the underlying EU4a is an evidence of the high shear rate exerted by the EU4b whose deposit can be interpreted as derived from a short-lived density stratified PDC.

2.1 AD 472 deposits

The AD 472 Pollena eruption was classified by Cioni et al. (2008) as a sub-Plinian type I event, distinguished from a sub-Plinian type II event based on size and magnitude (both higher for the sub-Plinian type I) and on the dispersal of PDC deposits (within 2/3 km and 8/9 km from the vent for the sub-Plinian type II and type I, respectively). The AD 472 Pollena eruption was characterized by volumetrically important PDCs (0.15 km^3; Sulpizio et al. 2007) and by a sustained phase which, unlike the Plinian case, is interpreted to have been dominated by an instability in magma discharge. Sulpizio et al. (2007) subdivided the eruption into three main eruptive phases according to inferred changes in the eruptive processes and/or changes in melt composition. The PDC deposits are associated with the last two eruptive phases, including the PDC deposits of unit F_g (Sulpizio et al. 2005), whose physical parameters have been here calculated. During the eruption, the formation of PDC might have been related to partial or total collapses of the convective column responsible for the deposition of the two preceding fallout units (L8 and L9; Sulpizio et al. 2005). Deposition of the F_g unit of the AD 472 Pollena eruption (Fig. 2c) was generally strongly controlled by topography, with massive to stratified, lapilli-bearing, ash- and lithic-rich deposits and only minor, cross-laminated to dune-bedded deposits. The thickness varies from a few tens of cm up to 7 m. Lithofacies in F_g units consist of massive, valley-ponded lapilli tuff with few examples of crudely stratified ash deposits at the bottom of this lithofacies (Sulpizio et al. 2007). Sedimentological features suggest that deposition occurred from a highly concentrated, granular to fluid-escape dominated underflow at the base of a thick, short-lived, rapidly depletive current (Sulpizio et al. 2007).

3. Datasets

Field data for each of the studied PDC deposits are here used for extracting quantitative physical parameters. We focus on the quantitative assessment of the following parameters and of their inherent uncertainties: (1) maximum runout distance; (2) flow invaded area; (3) volume of the deposit; (4) total grain size distribution of the PDC.

Because a standardized protocol is not available for the quantification of these parameters for PDC deposits, we compare results obtained through the application of different methods. Samples and measurements refer to a total of 243 stratigraphic sections (Fig. 3), either partially unpublished or taken from published studies (Cioni et al. 1992; Gurioli 1999; Gurioli et al. 1999; Tadini et al. 2017b). Data on stratigraphic sections, samples and density measurements of the deposits are available in the Supplementary Material section (Online Resources 1, 2, 3 and 4) and shown in Figure 3 and Online Resource 5. The three PDC deposits, which vary terms of transport and depositional mechanics, dispersal area and geometry and grain size, allow us to discuss the general applicability and reliability of the different methods and to compare the associated uncertainties.

4. Methods and Results

We first present the rationale and the methods used for estimating each different parameter and the related uncertainty, followed by the results for each deposit. We stress that each unit required different methods to estimate its parameters.

4.1 Maximum runout and invaded area

In this paper, maximum runout refers to the distance attained by a laterally moving current, and does not include, for example, distal co-ignimbrite ashfall layers. The problem of tracing the maximum runout of a PDC has not been previously addressed in detail (Burt et al. 2001). Recently, Gurioli et al. (2010) estimated the maximum runout of PDCs associated with Plinian and sub-Plinian eruptions at Somma-Vesuvius through the definition of two parameters: the farthest outcrop distance (the farthest point at which the PDC deposit can still be unambiguously identified); and the maximum runout (the theoretical distance covered by the PDC before it stopped). Ideally the two distances would coincide in the case the deposit is completely preserved and fully accessible to investigation. However, the authors underline also that in cases where the distribution of distal deposits is poorly constrained (particularly for the older eruptions), true maximum runout is likely is greater in distance than the most distal outcrop. To overcome this ambiguity in the definition of maximum runout, we suggest to: 1) position a line of maximum runout (MRL) that is based on field data and the sedimentological features of the deposits; 2) introduce an estimation of the uncertainty on MRL position, following a simplified procedure of expert judgement to reach consensus between different authors. A similar, simpler approach was adopted by Neri et al. (2015) by placing a buffer on the deposit boundary with constant range estimated by expert judgment.

We structured the procedure for the definition of the MRL (and of the related maximum invaded area - MIA) upon a sequence of spatial constraints. In particular, in order of decreasing relevance: i) the position of the minimum observed thickness of the deposit (as directly measured in the field); ii) the presence of topographic obstacles that could have limited PDC propagation area; iii) the general areal extent of still preserved deposits as derived from available geological maps; iv) the position of the stratigraphic sections still preserving deposits of the target eruption but which lack the deposits of the PDC of interest. Given the intrinsic uncertainty in defining the exact position of MRL, we adopt a procedure by which three different positions for the MRL are traced: a median (or "best guess") value of this parameter for the specific unit investigated (the 50^{th} percentile outline – MRL_{50}) and two uncertainty bounds (the 5^{th} and the 95^{th} percentiles, that are MRL_5 and MRL_{95}) that take into account the epistemic uncertainty associated with the incomplete knowledge of the deposit. In other words, while the MRL_{50} is defined through the critical analysis of the four different geologic constraints listed above, the MRL_5 and MRL_{95} percentile curves define an uncertainty belt for the maximum runout estimation and represent the lines having respectively 5% and 95% of probability not to have been overstepped by that PDC. MRL_{50} was traced at an average downcurrent distance no further than 500 m from those stratigraphic sections with the smallest measured thickness. When tracing the MRL_{50}, different segments of the line are distinguished and associated with sectors for which the available geological constraints on PDC runout have different degrees of confidence (Fig. 4).

Once defined, the segments (and sectors), for each of the upper and lower uncertainty bounds (respectively corresponding to the position of the MRL_5 and MRL_{95}) are evaluated. This is a significant novelty compared to the procedure applied by Neri et al. (2015), where the MRL and its uncertainties were defined without any preliminary distinction in segments. In this study, four different uncertainty bounds (in terms of distance from the MRL_{50}) were applied and linked to the maximum runout distance reached within the MRL_{50} for each unit. Low, moderate, moderate-high and high uncertainty were estimated in terms of a percentage of the distance with respect to the vent of the maximum runout distance of the MRL_{50}, and corresponding to, respectively, 10%, 5%, 2.5% and 1% of this distance. The distance between the MRL_5 and MRL_{95} is small in cases of sectors with strong geological constraints, while it is larger for those areas where few outcrops were observed. Conversely, the distance between the MRL_{50} and MRL_{95} lines has a maximum also for those

areas where the thickness of the deposit is more than 1 m (i.e., they do not represent the maximum runout of the PDC). For all these reasons, upper and lower uncertainty values for a single segment of the MRL_{50} might be the same (e.g. lower bound might be -200 m while the upper might be +1000 m with respect to the position of the MRL_{50}) depending on the number of constraints available.

The choice of the uncertainty bounds for each segment is based on a simplified "expert judgment" procedure among the authors of the paper. Although our approach is not structured, as in similar studies (e.g., Selva et al. 2012; Bevilacqua et al. 2015; Tadini et al. 2017a) it involved a detailed discussion about all the sources of uncertainty for each segment, detailed in the following, until a consensus was reached about the attribution of the uncertainty bounds. On the contrary, the uncertainty range was enlarged in cases of discordant views. Based on the comparison with the studies referenced above, we do not expect that involving other experts will have a large modification on the results, unless new data or assumptions are introduced into the discussion.

In summary, the MRL_5 always represents the line closest to the farthest (and thinnest) deposit measured in the field. MRL_{95} approximates the maximum expected runout of a given PDC, based on the critical consideration of all the geologic constraints that can be used in the expert judgement. In this study we provide three percentile constraints representing an unspecified probability distribution; this approach is a common practice in expert judgement techniques (although with differences in distribution types; Cooke 1991; Flandoli et al. 2011), but has been rarely adopted in spatial mapping problems (see for instance Bevilacqua et al. 2015; Neri et al. 2015; Bevilacqua 2016). Diagrams that illustrate the preferred directionality in the dispersal of the deposits are given in Fig. 6, where the variation of the distance from the vent of the MRL for the different studied deposits (and for each of the three isolines traced) is given as a function of the azimuthal angle with respect to the north. The definition of MRL (and related uncertainty) easily allows us to calculate the maximum invaded area (and related uncertainty – Table 1) as the area included within each single MRL.

4.1.1 AD 79 EU3pf

The maximum runout distance (MRL_{50}) for EU3pf is around 9 km, and therefore the low, moderate, moderate-high and high uncertainty values are, respectively, 90, 275, 450 and 900 m. The MRL_{50} is composed of three segments, each with different uncertainty (Fig. 5a) and identified in Figure 5a with different numbers. Part 1 of MRL_{50} corresponds to the segment toward the N, NE and SE with respect to the vent location. This segment is well constrained by numerous stratigraphic sections where EU3pf is only few centimeters thick, so that the uncertainty on MRL position is low (MRL_5 – 90m; MRL_{95} +90m). Part 2 of MRL_{50} represents the inland part toward NW. In this case, the constraints are represented by only a few stratigraphic sections located to the NNW, where the thickness of EU3pf is of the order of few meters, and the related uncertainty on the position of the MRL has been considered moderate to high (MRL_5 –275m; MRL_{95} +450m). Part 3 of MRL_{50} constitutes the seaward part. No constraints are available here except for a few stratigraphic sections near the coastline where thicknesses are of the order of several meters, making the related uncertainty notably high (MRL_5 -450m; MRL_{95} +900m). The MRL_{50} (Fig. 6) varies for the different sectors, passing from about 4 km for the eastern sector, to about 9 km for the south-eastern sector.

4.1.2 AD 79 EU4b

For the EU4b unit, the maximum runout distance of the MRL_{50} is 20 km, and therefore the low, moderate, moderate-high and high uncertainty values are, respectively, 200, 500, 1000 and 2000 m. The definition of the maximum runout for the EU4b unit is based on stratigraphic information and on paleo-topographical constraints. EU4c was not considered in terms of maximum runout as only a very small part of it can be related to deposition from a laterally moving, highly dilute current, whereas most of this unit was related to fallout deposition from a convective, co-ignimbritic plume. We have however performed a rough estimation of the area affected by deposition of unit EU4c (using information from Gurioli 1999) to be used in the following as the integration limit for the calculation of the total grain size distribution of the eruptive mixture (see section 4.3.2). In order to define the extent of the MRL_5 and MRL_{95}, the MRL_{50} of EU4b unit was divided into 4 different segments (Fig. 5b). Part 1 of MRL_{50}, representing the inland part toward S and SE, is associated with a narrow zone of uncertainty (MRL_5 –200m; MRL_{95} +200m), resulting from the presence of quite robust constraints onto the 10 cm isopach (Gurioli et al. 2010) and by the proximity of the MRL_{50} to the steep northern slopes of the Sorrento peninsula (to the SE) and of the Apennines (to the E). Part 2 of MRL_{50} corresponds to the seaward part. For this segment (which is has the highest uncertainty) there is evidence that the PDCs travelled at least 5-7 km across the sea, and reached the paleo-coastline of the Sorrento peninsula at the S. Maria di Pozzano site (section 203; see Figs. 3 and Online Resource 1). For this reason, the MRL_{50} in this sector has been placed at an average distance of 5 km off the coastline and associated with high uncertainty (MRL_5 –500m; MRL_{95} +2000m). Part 3 of MRL_{50} represents the inland part toward NW. No strong stratigraphic (nor topographic) constraints are present here; for these reasons, the uncertainty is moderate-high (MRL_5 –500m; MRL_{95} +1000m). Part 4 of MRL_{50} is constituted by the inland part toward N. A stronger constraint here is the position of the 10 cm isopach (Gurioli et al. 2010). As a consequence, uncertainty in maximum runout can be considered moderate in this sector (MRL_5 –200m; MRL_{95} +1000m). Maximum runout distance occurs in the ESE sector, where the PDC reached around 20 km from the vent, while in the northern sector, where the initial path of the PDC was possibly shielded by the high Mt. Somma scarp, the current travelled not farther than 7-8 km (Fig. 6).

4.1.3 AD 472 F_g

The F_g unit of the AD 472 Pollena eruption is dispersed in multiple lobes in different sectors of the volcano. In this study, two different lobes (i.e. the Cupa Fontana and Cupa Olivella; Fig. 5c) have been traced separately and used for the definition of the maximum runout. Due to the scarcity of measurable outcrops, several cross-sections were traced through points of measured thickness. Along the cross-sections, the thickness was extrapolated taking into account paleo-morphology of the substrate (as resulting from field observations) and assuming a horizontal upper surface of the deposit. Additional information was also derived from the geologic map of Sbrana et al. (2020). This resulted in a significantly larger set of measured and extrapolated data, used to constrain both isopachs and maximum runout isolines for the two lobes (Fig. 5c; the complete list of "Measured" versus "Interpolated" thicknesses is provided in Online Resource 4).

In contrast to the outlines traced with mainly unpublished data for the two AD 79 PDC units, the MRL_{50} was drawn by simply considering the outline of the preserved deposit of the AD 472 Pollena PDC units in this area. This approach was preferred over the previous one due the nature of the deposits that clearly derived from a highly concentrated, rapidly depletive current. Such currents generally pass to en-masse deposition at their distal ends, and terminate with steep-sided lobes up to decimeters thick (Branney and Kokelaar 2002). Thus, the farthest measured outcrop in this case is at the

same time a good approximation of both the best guess and the minimum value to be considered for runout. Consequently, the MRL_5 and the MRL_{50} are considered in this case as coincident. The MRL_{95} has been placed at a constant distance of +200 m with respect to the MRL_{50}, as the thicknesses of both the F_g Cupa Fontana and Cupa Olivella PDC lobes in the stratigraphic sections close to the MRL_{50} are of the order of only few centimeters. This distance corresponds to an uncertainty between moderate (2.5% of maximum runout distance within MRL_{50}) and moderate-high (10% of maximum runout distance within MRL_{50}), since the average MRL_{50} is in the range of 5 km from the vent (Fig. 6), both for the Cupa Fontana and the Cupa Olivella lobes.

4.2 Volume estimation

In contrast to large-volume PDC deposits (see for example Scarpati et al. 2014), estimating the volume of small- to intermediate-volume PDC deposits is a more difficult task, mainly because deposition from parent PDCs is more strongly controlled by preexisting topography and cannot be described through a general decay law of thickness that can be integrated over area (or distance). In addition, the volume of the PDC deposits does not coincide with the volume of the solid phase transported in the moving PDC, due to redistribution of fine material between the horizontally moving current and the associated co-ignimbrite plumes. However, the volume of the deposits provides the best proxy for calculating the solid mass transported by the PDC, as long as uncertainty is explicitly assessed (Sulpizio et al. 2005; Gurioli et al. 2010). Apart from a few examples (Isaia et al. 2004), there is still no general consensus about the best procedure for volume estimations of small-scale PDC deposits. To address this problem, in this work six different approaches (summarized in Table 2) have been used and the results compared to each other. Such approaches have been previously applied mainly to tephra fallout deposits (Pyle 1989; Fierstein and Nathenson 1992; Bonadonna and Houghton 2005; Bisson and Del Carlo 2013) and to debris avalanche deposits (Crandell 1989).

Table 3 reports the percentages of area (with respect to the total dispersal area) enclosed in the MRL_{50} which pertains to each of the three slope classes for all the PDC deposits here considered. Epistemic uncertainty on volume estimation is mainly based on the lack of direct knowledge about the real extent of the PDC dispersal. This uncertainty has been included in the following only for the case of the TIN method using the three different maximum runout lines (MRLs) defined for each unit, considering the area enclosed by the MRL_{50} as representative of the expected measure of deposit dispersal.

4.2.1 AD 79 EU3pf

The dataset used for volume calculations of EU3pf unit consisted of 106 stratigraphic sections (Online Resource 1), while information on 0 m thickness is extracted from the different MRLs. The areal coverage of stratigraphic sections is moderately dense in the northern sector, due to the presence of numerous valleys and road cuts. Using the thickness values, segments of three different isopachs were also drawn (Fig. 5a) and used for volume calculations.

Four different methods (CRh, CRs, VOR and TIN; Table 2) were used for estimating the volume of this unit; three of these (CRh, CRs, VOR) were used to calculate volume within the MRL_{50} only, while for TIN method the volume was calculated considering the deposit enclosed by the MRL_5, MRL_{50} and MRL_{95}, in order to estimate the uncertainty on the measure.

The sectors for the application of methods CRh and CRs were defined as follows: (1) for the CRh method, EU3pf deposit was divided into four areas, corresponding to different fans in the NW, NE, SE and SW sectors of the volcano (and mainly related to the paleotopography; Fig. 5a); (2) for the CRs method, EU3pf deposit was divided into three sectors using the three different slope classes defined in Table 3. The VOR method was applied to the total dataset of available thickness data. The uneven distribution of the points, and especially the lack of points in the proximal (less than 4 km distance from the vent) and in the eastern sectors, imply the tracing of very large Voronoi cells, resulting in a low reliability to the volume estimate. In the application of the TIN method, the EU3pf deposit was further subdivided into a northern and a southern zone (Fig. 5a) in order to account for the blocking effect of the Mt. Somma scarp, and separated volumes were calculated accordingly.

All volume estimations are shown in Table 4. With respect to the TIN estimations, it is evident how the two sectors (N and S) have substantially the same volume of deposit. Results show that the sectorialization CRs methods tend to produce volume estimates up to 40% higher with respect to the TIN method. Even larger estimates (50% larger with respect to the TIN method) derive from the use of VOR method. Uncertainty on volume estimation based on the TIN method (as calculated respect to the uncertainty on the invaded area) is slightly asymmetric with respect to the median value (-19% and +28%), and well below the differences with respect to the volume values obtained with the other methods.

4.2.2 AD 79 EU4

For the EU4 unit, volume was assessed in a detailed way only for EU4b (Table 5), as this is the only bed that can be directly related to deposition from a PDC. For this estimate, a total of 102 stratigraphic sections were used (Fig. 5b). Thickness data were used to trace 7 isopachs, from 0.1 m to 4 m (Fig. 5b). Volume of the EU4b unit was estimated following methods CRs, TR, PY, VOR and TIN (Table 2). An estimation on the volume for unit EU4c was also performed, in order to refine the calculation of the TGSD of the collapsing mixture (see section 4.3.2), and to estimate the relative amount of material. This estimation (0.034 km^3) was performed using the TIN method and the outline of Fig. 7c as integration limit.

As for the EU3pf, methods CRs and VOR give the highest volume estimates, respectively, of 90% and 70% higher with respect to the volume calculated using the TIN method. Volumes estimated with method TR and method PY (with two segments approximation) are only slightly higher (+24% and +15% respectively) than that from the TIN method. Due to the integration up to an infinite area of method PY, the result of this calculation could represent a maximum value for the volume of the deposit. Finally, the TIN method was applied to calculate the volume using points on the three MRLs as zero-thickness points, in order to have an estimation of the uncertainty related to the maximum dispersal area, which is however moderately low (Table 5). The small uncertainty in the calculation of volume derives from the continuous and nearly regular thinning with distance of the EU4b deposit, with low values of thickness measured at the most distal sites.

Because of the asymmetric dispersal of the EU4b deposits (the maximum runout distance for the southern quadrants is larger on average with respect to that for the northern quadrants; Figs. 5b and 6) the deposits have been subdivided into two distinct areas: NW and SE. These partitions were defined by drawing a straight line (dashed green line in Figs. 5b and 7b) perpendicular to the axis of maximum elongation of the deposit (oriented roughly NW-SE). Despite the larger area of the SE sector with respect to the NW, the volume results are more or less evenly distributed between the two

sectors (60% vs. 40%, respectively; Table 5), due to the generally lower thickness of the deposits of the SE sector, which is probably related to the gentler slope and lower topographic roughness.

4.2.3 AD 472 F_g

Volume estimations for the two F_g PDC lobes from the AD 472 Pollena eruption utilized a total of 27 stratigraphic sections (6 measured and 21 interpolated), and 31 sections (12 measured and 19 interpolated) for the Cupa Fontana and Cupa Olivella, respectively. Thicknesses range between 1 cm and 4.8 m. Volumes were calculated with methods CRs, VOR and TIN (Table 2), all referred to the $MRL_{5/50}$ (Table 6).

The deposits volumes for these very restricted lobes are small: an order of magnitude lower than those calculated for EU4b. This possibly reflects the lower intensity of this eruption with respect to the AD 79 eruption. Relative uncertainty in the estimate is related to the extent of the invaded area which was evaluated by comparing the volumes within the $MRL_{5/50}$ and the MRL_{95} with the TIN method. This uncertainty is however of similar magnitude to the two larger PDC deposits, and varies from 10% to 17% of the estimated volume (for the Cupa Fontana and Cupa Olivella lobes, respectively). As for the other two cases discussed above, the lower volume values are returned by the TIN method, while the use of the CRs method results in values nearly double those derived from the TIN method. The volume calculated with the VOR method gives higher, but largely variable, values with respect to the TIN method (30% and 80% respectively, for the two lobes). This is possibly related to the low number of sites available for measuring thickness in the field, which are generally restricted to the upstream part of the two lobes and have high thickness values.

4.3 Total Grain Size Distribution (TGSD)

The Total Grain Size Distribution (TGSD) of PDC deposits represents an important parameter for the understanding of physical processes involved in transport and deposition from these currents and for numerical modeling related to hazard assessment. In this study, we applied and compared two methods for TGSD calculation (Table 7): (1) the Voronoi tessellation method (Bonadonna and Houghton 2005), using as the integration limit the MRL_{50} for units EU3pf, EU4b and F_g (Fig. 7); (2) the Walker (1980) method (referred to from now on as "isomass method") integrating the resulting plot of mass per area for each grain size class Φ (M/A_{Φ}) vs. the square root of the area ($A^{1/2}$) of each isomass curve through the formula of Fierstein and Nathenson (1992). Grain size analyses were performed in the interval -4Φ to 5Φ at 1Φ interval. For stratigraphic sections with more than one sample, the average grain size of the section was calculated by averaging all the grain size analyses of samples collected at that section. Density values for the PDC deposits were directly measured on several samples. In the supporting information we are providing the following detailed data: (1) grain size analyses for all units (Online Resource 2); (2) deposit density measurements (Online Resources 3 and 4); (3) distribution of stratigraphic sections for all units (Online Resource 5); (4) TGSD numerical values and subpopulations data (Online Resource 6) and; (5) isomass maps for units EU4b and EU4c (Online Resources 7, 8, 9, 10). TGSD data are generally polymodal, and in many cases the classical grain size distribution parameters are not appropriate to fully describe the whole distribution. For this reason, TGSD data have been deconvoluted into multiple Gaussian subpopulations (SP) using the SFT software (Wohletz et al. 1989), and for each subpopulation the median value, the standard deviation and percent by weight with respect to the total sample have been calculated. Due to the lower limit of the sieving (5Φ), one SP was arbitrarily

placed around this diameter, and the median value of this should be considered as "finer than 5Φ". In the studied examples, this fine-grained SP represents from 1 to 15 % of the total.

The calculated TGSDs for the PDC deposits, whatever the method used, are only representative of the lapilli to coarse ash fractions of the original pyroclastic mixture carried by the PDC. Estimation of the finer-grained fractions is complication by elutriated by ash production by clast comminution and abrasion during the transport. Here, we attempted to estimate the contribution to the TGSD of the elutriated ash deposited from the co-ignimbrite cloud for the EU4 unit using data for EU4c sub-unit. Table 7 summarizes the information related to TGSD estimation for all the studied units.

4.3.1 AD 79 EU3pf

TGSD was calculated for this unit only using the Voronoi method, as no simple fit was possible on an ln M/A_{Φ} vs. $A^{1/2}$ plot for using the "isomass method". As in the case of the volume calculation, TGSD was calculated both for the total deposit (Fig. 7a), and for the N and S sectors (separated by the green dashed line of Fig. 5b) for the same reasons. TGSD for the different sectors are however nearly coincident (Fig. 8a), the main difference being related to a larger (around 5%) amount of fine ash ($\Phi > 5$) in the deposits dispersed to the south. Resulting total TGSD is nearly unimodally distributed, with a main mode at 0.5Φ representing around 92 % of the total (Online Resource 6). F1 value (wt. % of ash finer than 0 Φ; Walker 1983) is around 40 %, while F2 (wt. % of ash finer than 4 Φ; Walker, 1983) is slightly more than 10 %.

4.3.2 AD 79 EU4

EU4 represents an unusual case in which both the deposits of a PDC (EU4b unit) and those of the associated co-ignimbrite cloud (EU4c unit) can be recognized and mapped in the field. For this reason, it was possible to estimate the TGSD for the two units, the weighted sum of which (EU4b/c) can be considered a good approximation of the TGSD of the pyroclastic material in the collapsing column. The distribution of the sections and the related Voronoi polygons used for the TGSD estimations for EU4b and EU4c are shown in Fig. 7b and 7c respectively.

TGSD with the Voronoi method for the EU4b unit is shown in Fig. 8b, both for the whole deposit and for the NW and SE sectors. The results from the two sectors are very different, with TGSD for the SE sector being more fines-rich compared to the NW sector: the value of F1 in the SE is nearly double respect to that in the NW). When integrated with respect to the mass distributed over the two sectors, the TGSD results are strongly platykurtic and polymodal.

The comparison of TGSD of EU4b (Fig. 9) calculated with the different methods suggests that: (1) the Voronoi tessellation method tends to estimate a lower amount of fine materials with respect to the isomass methods; (2) the estimations, performed by integrating different approaches to the isomass maps, show an irregular distribution with a marked polymodality (4 main subpopulations; Online Resource 6).

The dispersal outline used for tracing the isomass maps is the same used in section 4.2.2 for volume calculations. TGSD is strongly asymmetric, with a main mode between 2.5 and 3.8Φ (Online Resource 6) and more than 90 wt% of ash finer than 0 Φ. The total mass of EU4c, which represents around 10% of the mass of EU4b, was calculated by multiplying the mean density of the deposit (Table 7) by the estimated volume of EU4c (see section 4.2.2). Summing up the TGSD data of EU4b and EU4c units, after weighing for their total mass, we obtained a TGSD (EU4b/c) that can be considered representative of the distribution of the erupting mixture ejected from the vent. This latter is characterized by a very poorly sorted, polymodal distribution, with at least 4 subpopulations (Fig. 9c; Online Resource 6). With respect to the TGSD of

Fig. 9, it should be specified that at the current stage the position of the mode at the Φ=5 size should be considered an artifact, as data for the Φ=5 class represent a total of all the grain sizes finer than that class.

4.3.3 AD 472 F_g

Given the limited dispersal and the very similar facies characteristics of the deposits throughout their dispersal, the TGSD for the Cupa Fontana and the Cupa Olivella lobes was tentatively estimated only through the Voronoi method (Fig. 7d).

TGSD for both of the lobes are shown in Fig. 8c. It is evident the similar modal value for the two lobes (between 0 and -0.6 Φ; Table 5SM), and the more fines-rich nature (F1=32%) of the Cupa Olivella with respect to the Cupa Fontana lobe (F1=23%), are possibly related to the availability of samples from more distal sites in the former (Fig. 7d).

5. Discussion

Estimating the natural variability and related uncertainties of physical parameters like maximum runout distance, volume, and total grain size distribution of PDC deposits is complicated due to the intrinsic variability of dispersal and sedimentological characteristics. Any study with these goals must begin with a detailed field analysis of the lithofacies associations in the deposits (Branney and Kokelaar 2002; Sulpizio and Dellino 2008), in order to select the most appropriate methods for the calculation of these parameters. Many field measurements (thickness of different units, density of the deposit) and samples should be collected, especially from areas where the PDC was emplaced over rugged paleotopography. The three cases discussed above for Somma-Vesuvius represent a range of PDC types, allowing us to infer the main factors controlling their main parameters (volume, invaded area, runout distance and TGSD), to statistically compare the methods for their estimation, and to quantify, for the first time, a comprehensive range of these parameters for different PDC deposits that will be useful for future application of numerical models and hazard assessments at the volcano. We think that the goal of a robust reconstruction of the properties of past PDC is not in contradiction with the presence of uncertainty and it should deal with it specifically.

5.1 MRL and MIA estimations

Estimation of maximum runout and invaded area (MRL and MIA, respectively) define the possible area impacted by a PDC. Several considerations can be made with respect to the methods for the definition of the maximum runout outlines of past events based on incomplete stratigraphic records. While the occurrence at distal sites of thin PDC deposits can be used for assessing minimum runout distances, it is difficult to constrain the distance at which the related PDC actually stopped and/or lifted off based solely on deposit evidence (Andrews and Manga 2011). Thus, the rationale used for constraining MRL and MIA varies on a case by case base.

The topography surrounding Somma-Vesuvius exerts a first-order control on maximum runout. This is especially true in the case of PDCs with a runout of at least 10 km where low values of the thickness of the deposit coincide with the onset of a positive gradient in the local topography. Areas with the highest degree of uncertainty in maximum runout are those located in sectors where stratigraphic information is confined to proximal sites or where the PDCs entered the sea. Documented cases elsewhere show that PDCs can either travel long distances over the water, or stop rapidly (Carey et al. 1996; Cole et al. 1998). The presence of EU4b deposits on the northern side of the Sorrentina peninsula (Figs. 1 and 3;

Cioni et al. 1992) is direct evidence of the ability of the PDC to travel over the sea for at least 7-8 km, passing across the Gulf of Napoli (Fig. 1). Evidence for dense, granular PDCs entering the sea is reported for the AD 1631 sub-Plinian eruption (Rosi et al. 1993): numerous paintings (e.g. Giovan Battista Passeri, "Vero disegno dell'incendio del mons Vesuvii 1631") illustrate PDCs stopping only a few hundred meters after entering the sea. Definition of the maximum invaded area and hence of the maximum runout lines for this side of the volcano for our study cases is consequently largely inferred. Since in all these cases there is a large uncertainty in the position of MRL, the need for a quantitative range justifies the application of expert judgement techniques to deal with it (Neri et al. 2014, 2015).

Additional information for the definition of the maximum runouts and of their uncertainties could be derived from observations on PDC deposits. For those related to concentrated PDCs (AD 472 F_g), topography was the main controlling factor on their dispersal, and topographic features could be used to constrain maximum runouts. For deposits of dilute PDCs (AD 79 EU3pf and EU4b), the steep decrease of thickness with distance implies that the presence of thin (less than 10 cm thick) massive, ash-dominated deposits at distal sites can be interpreted as good evidence of proximity to the maximum runout distance, with a consequent lower uncertainty in its definition.

In the absence of direct data, and associated uncertainty, the use of different limits representing the reconstructed maximum runout distance assessed in probabilistic terms (MRL_5, MRL_{50}, and MRL_{95}) appears an effective way to quantify the uncertainty on the estimate of this parameter. The position of the upper and lower uncertainty bounds are more amenable to expert judgement.

As a consequence of large uncertainty in estimating maximum runout, estimates of the invaded area (MIA) are also uncertain. The selected examples entail a wide variation, with MIAs varying from less than 10 km^2 (in case of AD 472 F_g lobes) up to more than 500 km^2 (in the case of AD 79 EU4b). Uncertainty is generally not symmetric with respect to the reference value (MIA corresponding to the MRL_{50}), and is generally lower for the lower bound (varying from 0 to 14% relative) and larger for the upper bound (from 14 to 30%). Total uncertainty on area is however estimated around 15-20% for the two small lobes of F_g, while it varies between around 25 and 40% for the widespread deposits related to turbulence-dominated PDC (EU3pf, EU4b). We suggest that these percentages should be considered as first-order reference values for uncertainty when assessing the area invaded by a PDC, especially in studies related to emergency planning.

5.2 Volume estimation

The evaluation of the volume of a PDC deposit is the first, necessary step to define the mass of magma (and possibly non-juvenile material) dispersed by a PDC and is a fundamental parameter needed to physically describe and realistically model the current. The volumes of the different PDC deposits examined here have been estimated using different approaches, and their comparison can provide preliminary estimates of the method-related uncertainty. Due to the non-regular spatial thickness variability of PDC deposits, the different approaches give in general quite different results, due to the implicit differences in the area integration of thickness data. The TIN method represents a simpler way of extrapolating thickness on the basis of a randomly spaced dataset of measured points. This is an advantage in the absence of theoretical models able to derive a physical law for thickness variation with distance. In particular, the TIN method can be also enhanced if, in addition to the measured data, inferred/hypothetical data can be added to the available dataset, based on the observation of the paleotopography and some basic assumptions on the geometry of PDC deposits (see data used for F_g unit). However, the comparison of TIN with other methods is a key to the estimation of the related uncertainty. In particular,

we observe that: a) the CRh and CRs methods generally result in the largest volume estimations, since the mean thickness values attributed to each sector are generally skewed toward higher values (thick deposits are better preserved than thin ones); b) the VOR method tends to reduce the thickness variation of the deposit (since it creates polygons with a constant thickness), resulting in a poorly controlled variability of the total volume, especially in the presence of a low number of measured sites and rugged basal topography; c) due to the difficulty of tracing isopach maps for PDC deposits (dispersal is generally heavily irregular), also data derived from the TR method tend to be biased toward high values, however its results are more similar to those of the TIN method. Similarly to the trapezoidal rule, the PY method can give results that well agree with those derived from TIN, but in this case it is fundamental to trace an isopach with an arbitrarily low value of thickness (however different from 0, we suggest here, by reference, a 1 mm thickness) in coincidence with the position of MRL. A very large envelope of the method-related uncertainty is derived for the PDC volume (from 50 to 100% respect to the output of the TIN method). In addition, considering only the TIN method, we estimated the effects over the volume value of the epistemic uncertainty in the extent of dispersal area (i.e. the MRL_5 and MRL_{95}, as discussed for the evaluation of the maximum runout). In this case, the total uncertainty is generally lower, and is placed between 10% and a maximum of 45%. We note that such uncertainty is lower for deposits that show a sharp decrease in thickness with distance (in our case EU4b), for which the large uncertainty in the definition of the invaded area does not reverberate with the same weight on the uncertainty in the volume (as thickness associated to the uncertainty belt around the MRL_{50} is low). Conversely, where thickness is poorly correlated with distance, the uncertainty is larger. We can therefore conclude, similarly to the maximum runout case, that the identification and measurement in the field of thin distal deposits is a fundamental requirement for robustly constraining volume estimates.

The volume of material initially transported by a PDC is different from the volume of its deposit. This is because a portion of the finer-grained pyroclasts are transferred into the convective, co-ignimbrite plume and are ultimately deposited as fallout material. The estimation of this part of the deposit is always problematic, as co-ignimbrite material is both mixed in the upper portion of the PDC-related deposit or has a largely different dispersal respect to the PDC deposit. The partitioning of pyroclasts between the PDC and its co-ignimbrite cloud are strongly related to PDC dynamics and initial ash content (Engwell et al. 2016). The AD 79 EU4 unit represents a good case for trying to estimate the relative amount of co-ignimbrite material associated with this PDC, as the co-ignimbrite ash deposits of the EU4c unit can be mapped. Results suggest that the material associated with this unit is at least around 10% (Table 5) of the volume of the PDC deposit: this is consistent with similar estimates derived from multiphase flow modeling of PDCs (e.g. Neri et al. 2002; Di Muro et al. 2004). The value calculated for the EU4 unit should be considered as an order of magnitude indication of the possible release of fine material to the atmosphere from a turbulent, diluted PDC of intermediate volume.

5.3 TGSD estimations

Despite the importance of this eruption source parameter for the application of several numerical models describing PDC dynamics, TGSD data for PDC deposits are generally not available in the literature due to the large variability of the grain size features of PDC deposits and to the sometimes erratic and spatial variability of thickness. Even when obtained, deriving TGSD from the integration over the entire deposit is not guaranteed to obtain a true representation of the initial TGSD of the pyroclastic mixture for three main reasons: i) coarse, proximal deposits are often under-represented by exposures or by the blockage effects of topographic obstacles such as caldera rims like at Somma-Vesuvius

(Valentine et al. 2019; Valentine 2020); ii) part of the finer-grained material present in the erupting mixture is not deposited by the PDC, and instead is incorporated into the buoyant part of the PDC and redistributed over by atmospheric advection and fallout deposition; iii) the grain size distribution of solid material carried in the current is continuously modified by abrasion and breakage of particles during transport (Manga et al. 2011; Kueppers et al. 2012; Mueller et al. 2016). These latter two processes are difficult to model accurately or describe quantitatively, and therefore TGSD data extracted from deposits should be considered as only a first order approximation of the initial TGSD.

From the discussion above, it is clear that in the estimate of the TGSD of a PDC there are different sources of epistemic uncertainty, and we suggest therefore that the usage of different methods for the estimation of the TGSD is the most efficient way to derive a first order estimate for TGSD (and hence of its uncertainty).

The data reported in this paper are therefore mainly addressed to quantify (and whenever possible, to reduce) the first source of uncertainty and, although they present large limitations, they still reveal significant differences in the initial TGSD for the deposits of different types of PDCs, that can be useful for modeling purposes.

Data on AD 79 EU4 unit allow us to discuss the underestimation of the fine-grained portion implicit in these TGSD estimations. From the presented results, the co-ignimbritic material represents around 10% of the total mass involved in the PDC formation, and the contribution of this mass (dominated by fine-grained material) to the TGSD of the whole PDC is changes it into a strongly platykurtic, poorly sorted distribution without any prominent modal class. To help constrain numerical modeling of PDC generation more data of this type should be derived for other units with different sedimentological features, whenever it is possible to trace the dispersal of both the PDC and the associate co-ignimbrite deposits.

5.4 Numerical modeling of PDCs and applicability of the proposed approach

The data here presented, and especially the proposed comparative approach to estimate MRL, invaded area, volume or TGSD for the different types of PDC from Somma-Vesuvius, is useful for defining the main input parameters for the physical modeling of such events, and for ascribing uncertainty ranges to such parameters which are critical for probabilistic, hazard-oriented studies (see for instance Tierz et al. 2018). The large variability of basic assumptions or general complexity of physical models for PDC (Roche et al. 2013; Dufek et al. 2015) reflects the different input data needed for their initialization or calibration. In particular, MRLs is an important parameter used to calibrate simplified kinetic models (energy cone, Malin and Sheridan 1982; Aravena et al. 2020; box-model, Esposti Ongaro et al. 2016), by applying match procedures to areal extent (Tierz et al. 2016) or maximum runout limits. The proposed methodology for the estimation of the associated uncertainty is of importance for these very simplified models, as uncertainty propagates into the final hazard maps largely by contributing to the define extents of the areas with different probabilities of invasion. In addition, volume, sometimes together with MRL, is a basic parameter to initialize either kinetic or depth-averaged models (VolcFlow, Kelfoun and Druitt 2005; Gueugneau et al. 2020; TITAN2D, Patra et al. 2005, 2020) and, despite the uncertainty in its calculation (see section 5.3), even TGSDs might be employed efficiently within numerical models. In particular, TGSD could be either used whole for some models (Biagioli et al. 2019; Aravena et al. 2020) or to derive representative grain size parameters such as, the Sauter mean diameter (Breard et al. 2019; Valentine 2020).

The approach presented here has been tested on a large, but not completely exhaustive, spectrum of PDC deposits, so that it can be taken as a first reference for the definition of such parameters at other volcanoes. The approach can be

enlarged, without applying substantial modifications, to comprise other types of deposits. As an example, MRL or volume of very coarse grained PDC deposits, like classical block-and-ash flow deposits not specifically considered here, could be estimated using an approach similar to that used for the channelized lobes of the AD 472 eruption. Conversely, TGSD estimates for these type of deposits would need a more accurate consideration of the coarse material, which could be done, for example, by integrating the results of dedicated image analyses techniques (Sarocchi et al. 2011). More importantly, the proposed approach also allows a more direct comparison of parameters like volume or TGSD of PDC with those of fallout deposits, for which well-defined procedures are already realized. This would enable a complete quantitative description of the deposits of complex, multiphase explosive eruptions (Sulpizio et al. 2005).

Our data clearly demonstrate the need for the collection of a detailed dataset of volcanological and sedimentological characteristics of different types of PDC deposits at a volcano to reach a breakthrough in the quantification of the main physical parameters which can characterize the PDCs. While it is clear that this is not possible at every volcano, the results from Somma-Vesuvius could help a first approximation of the level of uncertainty related with the estimation of these parameters elsewhere.

6. Conclusions

Parameters related to PDC deposits and relevant to physical modeling and numerical simulation of PDCs have been estimated and discussed in detail using a large dataset on the deposits of different types of PDCs at Somma-Vesuvius volcano. These parameters are maximum runout distance (MRL), maximum invaded area (MIA), volume, and total grain size distribution (TGSD). The lack of protocols for the estimation of these parameters has been here overcome by using different approaches and comparing and discussing the results obtained by different methods to extract the absolute value and related uncertainties of these parameters. This multiple approach currently represents the best way to extract a range of reliable values of all these parameters. The large variability of the inferred physical properties of the different PDCs considered here, whose deposits were dispersed over similar topography, permit first comparison of the natural variability of these eruptive parameters. In addition, the moderately large variability in dispersal area, volume, lithology and transport processes of the studied cases allow us to draw some general conclusions that are useful for the derivation of established protocols of calculation for the different parameters of small- to intermediate-scale PDC deposits.

The main results derived from the study are: (1) the uncertainty in the definition of the maximum runout line can be expressed by using three different reference isolines (MRL_5, MRL_{50}, and MRL_{95}), whose positions were defined by using non-formalized expert judgement pooling; (2) the extension of Maximum Invaded Area (MIA) and related uncertainty are directly derived from the different MRLs traced for a given deposit. For the Somma-Vesuvius case, the uncertainty on the invaded areas is quite high (up to 40% of the area related to the MRL_{50}), and this should be kept in mind for hazard assessment; (3) the volume of PDC deposits is hard to estimate due to the lack of regularity of thickness with distance from the eruptive vent. By adopting the TIN method and by using the uncertainty on the invaded area to estimate the uncertainty on volume, it is possible to derive an uncertainty in the range 10-45% of the median volume estimate. Lower uncertainties are associated with deposits showing a marked decrease of thickness with distance; (4) TGSD has been here estimated using the two main approaches already in use for fallout deposits (i.e. the Voronoi and isomass methods). Results are largely variable in terms of relative amount of single grain size classes, and the comparison of the two methods can provide a

general trend of the TGSD. In the studied units, co-ignimbrite deposits have been estimated to account for around 10% of the total mass involved in the PDC formation, an amount that can strongly modify the final TGSD estimation.

The numerical estimates and associated uncertainties obtained in this paper for three different types of PDCs at Somma-Vesuvius, represent the first attempt to constrain some of the most important parameters characterizing PDC formation and deposition, and should be used in the future as input data for hazard assessment studies at the volcano. We hope our approach could be strengthened by applying it to other volcanoes once new field data are available. Future work needs to address several unresolved issues, such as the mobility of PDCs above water (and therefore the maximum runout for the seaward parts of PDC deposits), the decay trend of thicknesses with distance (with implications for volume calculations) and the link between the TGSD calculated from deposit data and the initial TGSD erupted from the volcanic vent (with strong implications for numerical modelling).

References

Andrews BJ, Manga M (2011) Effects of topography on pyroclastic density current runout and formation of coignimbrites Geology 39:1099-1102 doi:https://doi.org/10.1130/G32226.1

Aravena A, Cioni R, Bevilacqua A, de' Michieli Vitturi M, Esposti Ongaro T, Neri A (2020) Tree-branching based enhancement of kinetic energy models for reproducing channelization processes of pyroclastic density currents Journal of Geophysical Research: Solid Earth doi:https://doi.org/10.1029/2019JB019271

Baxter PJ, Boyle R, Cole PD, Neri A, Spence R, Zuccaro G (2005) The impacts of pyroclastic surges on buildings at the eruption of the Soufrière Hills volcano, Montserrat Bulletin of volcanology 67:292-313 doi:https://doi.org/10.1007/s00445-004-0365-7

Bevilacqua A, Isaia R, Neri A, Vitale S, Aspinall WP, Bisson M, Flandoli F, Baxter PJ, Bertagnini A, Esposti Ongaro T, Iannuzzi E, Pistolesi M, Rosi M (2015) Quantifying volcanic hazard at Campi Flegrei caldera (Italy) with uncertainty assessment: I. Vent opening maps Journal of Geophysical Research: Solid Earth doi:https://doi.org/10.1002/2014JB011775

Bevilacqua A (2016) Doubly stochastic models for volcanic vent opening probability and pyroclastic density current hazard at Campi Flegrei caldera. PhD, Scuola Normale Superiore

Bevilacqua A, Neri A, Bisson M, Esposti Ongaro T, Flandoli F, Isaia R, Rosi M, Vitale S (2017) The effects of vent location, event scale, and time forecasts on pyroclastic density current hazard maps at Campi Flegrei caldera (Italy) Frontiers in Earth Science 5:72 doi:https://doi.org/10.3389/feart.2017.00072

Biagioli G, Bevilacqua A, Esposti Ongaro T, de' Michieli Vitturi M (2019) PyBox: a Python tool for simulating the kinematics of Pyroclastic density currents with the box-model approach Reference and User's Guide. doi:http://doi.org/10.5281/zenodo.2616551

Biass S, Scaini C, Bonadonna C, Folch A, Smith K, Höskuldsson A (2014) A multi-scale risk assessment for tephra fallout and airborne concentration from multiple Icelandic volcanoes-Part 1: Hazard assessment Natural Hazards and Earth System Sciences 14:2265 doi:10.5194/nhess-14-2265-2014

Bisson M, Del Carlo P (2013) A GIS-based application for volume estimation and spatial distribution analysis of tephra fallout: a case study of the 122 BC Etna eruption Annals of Geophysics 56:0105 doi:https://doi.org/10.4401/ag-6144

Bonadonna C, Houghton BF (2005) Total grain-size distribution and volume of tephra-fall deposits Bulletin of Volcanology 67:441-456 doi:https://doi.org/10.1007/s00445-004-0386-2

Branney MJ, Kokelaar BP (2002) Pyroclastic density currents and the sedimentation of ignimbrites vol 27. Memoirs. Geological Society, London

Breard ECP, Jones JR, Fullard L, Lube G, Davies C, Dufek J (2019) The Permeability of Volcanic Mixtures—Implications for Pyroclastic Currents Journal of Geophysical Research: Solid Earth 124:1343-1360 doi:https://doi.org/10.1029/2018JB016544

Burt ML, Wadge G, Curnow RN (2001) An objective method for mapping hazardous flow deposits from the stratigraphic record of stratovolcanoes: a case example from Montagne Pelée Bulletin of volcanology 63:98-111 doi:https://doi.org/10.1007/s004450100128

Carey S, Sigurdsson H, Mandeville C, Bronto S (1996) Pyroclastic flows and surges over water: an example from the 1883 Krakatau eruption Bulletin of Volcanology 57:493-511 doi:https://doi.org/10.1007/BF00304435

Cioni R, Marianelli P, Sbrana A (1992) Dynamics of the AD 79 eruption: Stratigraphic, sedimentological and geochemical data on the successions from the Somma-Vesuvius southern and eastern sectors Acta Vulcanologica 2:109-123

Cioni R, Gurioli L, Lanza R, Zanella E (2004) Temperatures of the AD 79 pyroclastic density current deposits (Vesuvius, Italy) Journal of Geophysical Research: Solid Earth 109 doi:https://doi.org/10.1029/2002JB002251

Cioni R, Bertagnini A, Santacroce R, Andronico D (2008) Explosive activity and eruption scenarios at Somma-Vesuvius (Italy): towards a new classification scheme Journal of Volcanology and Geothermal Research 178:331-346 doi:https://doi.org/10.1016/j.jvolgeores.2008.04.024

Cole PD, Calder ES, Druitt TH, Hoblitt RP, Robertson R, Sparks RSJ, Young SR (1998) Pyroclastic flows generated by gravitational instability of the 1996–97 lava dome of Soufriere Hills Volcano, Montserrat Geophysical Research Letters 25:3425-3428 doi:https://doi.org/10.1029/98GL01510

Cooke RM (1991) Experts in uncertainty: opinion and subjective probability in science

Crandell DR (1989) Gigantic debris avalanche of Pleistocene age from ancestral Mount Shasta volcano, California, and debris-avalanche hazard zonation USGS Bullettin

Di Muro A, Neri A, Rosi M (2004) Contemporaneous convective and collapsing eruptive dynamics: the transitional regime of explosive eruptions Geophysical research letters 31 doi:10.1029/2004GRL019709

Druitt TH (1998) Pyroclastic density currents Geological Society, London, Special Publications 145:145-182 doi:https://doi.org/10.1144/GSL.SP.1996.145.01.08

Dufek J, Esposti Ongaro T, Roche O (2015) Pyroclastic density currents: processes and models. In: Sigurdsson H, Houghton BF, McNutt SR, Rymer H, Stix J (eds) The encyclopedia of volcanoes. Academic Press, pp 617-629. doi:https://doi.org/10.1016/B978-0-12-385938-9.00035-3

Engwell SL, de'Michieli Vitturi M, Esposti Ongaro T, Neri A (2016) Insights into the formation and dynamics of coignimbrite plumes from one- dimensional models Journal of Geophysical Research: Solid Earth 121:4211-4231 doi:10.1002/2016JB012793

Esposti Ongaro T, Clarke AB, Voight B, Neri A, Widiwijayanti C (2012) Multiphase flow dynamics of pyroclastic density currents during the May 18, 1980 lateral blast of Mount St. Helens Journal of Geophysical Research: Solid Earth (1978–2012) 117

Esposti Ongaro T, Orsucci S, Cornolti F (2016) A fast, calibrated model for pyroclastic density currents kinematics and hazard Journal of Volcanology and Geothermal Research doi:https://doi.org/10.1016/j.jvolgeores.2016.08.002

Fierstein J, Nathenson M (1992) Another look at the calculation of fallout tephra volumes Bulletin of Volcanology 54:156-167 doi:https://doi.org/10.1007/BF00278005

Flandoli F, Giorgi E, Aspinall WP, Neri A (2011) Comparison of a new expert elicitation model with the Classical Model, equal weights and single experts, using a cross-validation technique Reliability Engineering & System Safety 96:1292-1310 doi:https://doi.org/10.1016/j.ress.2011.05.012

Gueugneau V, Kelfoun K, Charbonnier SJ, Germa A, Carazzo G (2020) Dynamic and impacts of the May 8th, 1902 pyroclastic current at Mount Pelée (Martinique): new insights from numerical modelling Frontiers in Earth Science doi:10.3389/feart.2020.00279

Gurioli L (1999) Flussi piroclastici: classificazione e meccanismi di messa in posto. PhD thesis, University of Pisa

Gurioli L, Cioni R, Bertagna C (1999) I depositi di flusso piroclastico dell'eruzione del 79 dC caratterizzazione stratigrafica, sedimentologica e modelli di trasporto e deposizione Atti Soc Tosc Sci Nat Mem Serie A 106:61-72

Gurioli L, Pareschi MT, Zanella E, Lanza R, Deluca E, Bisson M (2005) Interaction of pyroclastic density currents with human settlements: evidence from ancient Pompeii Geology 33:441-444

Gurioli L, Zanella E, Pareschi MT, Lanza R (2007) Influences of urban fabric on pyroclastic density currents at Pompeii (Italy): 1. Flow direction and deposition Journal of Geophysical Research: Solid Earth 112 doi:https://doi.org/10.1029/2006JB004444

Gurioli L, Sulpizio R, Cioni R, Sbrana A, Santacroce R, Luperini W, Andronico D (2010) Pyroclastic flow hazard assessment at Somma–Vesuvius based on the geological record Bulletin of Volcanology 72:1021-1038 doi:https://doi.org/10.1007/s00445-010-0379-2

Isaia R, D'Antonio M, Dell'Erba F, Di Vito MA, Orsi G (2004) The Astroni volcano: the only example of closely spaced eruptions in the same vent area during the recent history of the Campi Flegrei caldera (Italy) Journal of Volcanology and Geothermal Research 133:171-192 doi:https://doi.org/10.1016/S0377-0273(03)00397-4

Kelfoun K, Druitt TH (2005) Numerical modeling of the emplacement of Socompa rock avalanche, Chile Journal of Geophysical Research: Solid Earth 110 doi:https://doi.org/10.1029/2005JB003758

Kueppers U, Putz C, Spieler O, Dingwell DB (2012) Abrasion in pyroclastic density currents: insights from tumbling experiments Physics and Chemistry of the Earth, Parts A/B/C 45:33-39 doi:https://doi.org/10.1016/j.pce.2011.09.002

Malin MC, Sheridan MF (1982) Computer-assisted mapping of pyroclastic surges Science 217:637-640 doi:10.1126/science.217.4560.637
Manga M, Patel A, Dufek J (2011) Rounding of pumice clasts during transport: field measurements and laboratory studies Bulletin of Volcanology 73:321-333 doi:https://doi.org/10.1007/s00445-010-0411-6
Mueller SB, Kueppers U, Ayris PM, Jacob M, Dingwell DB (2016) Experimental volcanic ash aggregation: Internal structuring of accretionary lapilli and the role of liquid bonding Earth and Planetary Science Letters 433:232-240 doi:https://doi.org/10.1016/j.epsl.2015.11.007
Neri A, Di Muro A, Rosi M (2002) Mass partition during collapsing and transitional columns by using numerical simulations Journal of Volcanology and Geothermal Research 115:1-18 doi:https://doi.org/10.1016/S0377-0273(01)00304-3
Neri A, Aspinall WP, Cioni R, Bertagnini A, Baxter PJ, Zuccaro G, Andronico D, Barsotti S, Cole PD, Esposti Ongaro T (2008) Developing an event tree for probabilistic hazard and risk assessment at Vesuvius Journal of Volcanology and Geothermal Research 178:397-415 doi:https://doi.org/10.1016/j.jvolgeores.2008.05.014
Neri A, Esposti Ongaro T, Voight B, Widiwijayanti C (2014) Pyroclastic density current hazards and risk Volcanic Hazards, Risks and Disasters:109-140 doi:https://doi.org/10.1016/B978-0-12-396453-3.00005-8
Neri A, Bevilacqua A, Esposti Ongaro T, Isaia R, Aspinall WP, Bisson M, Flandoli F, Baxter PJ, Bertagnini A, Iannuzzi E (2015) Quantifying volcanic hazard at Campi Flegrei caldera (Italy) with uncertainty assessment: II. Pyroclastic density current invasion maps Journal of Geophysical Research: Solid Earth doi:https://doi.org/10.1002/2014JB011776
Patra AK, Bauer AC, Nichita CC, Pitman EB, Sheridan MF, Bursik MI, Rupp B, Webber A, Stinton AJ, Namikawa LM (2005) Parallel adaptive numerical simulation of dry avalanches over natural terrain Journal of Volcanology and Geothermal Research 139:1-21 doi:https://doi.org/10.1016/j.jvolgeores.2004.06.014
Patra AK, Bevilacqua A, Safei AA Analyzing Complex Models using Data and Statistics. In: International Conference on Computational Science, 2018. Springer, pp 724-736. doi:https://doi.org/10.1007/978-3-319-93701-4_57
Patra AK, Bevilacqua A, Akhavan-Safaei A, Pitman EB, Bursik MI, Hyman D (2020) Comparative analysis of the structures and outcomes of geophysical flow models and modeling assumptions using uncertainty quantification Frontiers in Earth Science doi:10.3389/feart.2020.00275
Pyle DM (1989) The thickness, volume and grainsize of tephra fall deposits Bulletin of Volcanology 51:1-15 doi:https://doi.org/10.1007/BF01086757
Roche O, Phillips JC, Kelfoun K (2013) Pyroclastic density currents. In: Fagents SA, Gregg TKP, Lopes RMC (eds) Modeling Volcanic Processes: The Physics and Mathematics of Volcanism. Cambridge University Press,
Rosi M, Principe C, Vecci R (1993) The 1631 Vesuvius eruption. A reconstruction based on historical and stratigraphical data Journal of Volcanology and Geothermal Research 58:151-182 doi:https://doi.org/10.1016/0377-0273(93)90106-2
Rutarindwa R, Spiller ET, Bevilacqua A, Bursik MI, Patra AK (2019) Dynamic probabilistic hazard mapping in the Long Valley Volcanic Region CA: integrating vent opening maps and statistical surrogates of physical models of pyroclastic density currents Journal of Geophysical Research: Solid Earth
Santacroce R, Sbrana A (2003) Geological map of Vesuvius. SELCA Firenze
Sarocchi D, Sulpizio R, Macías JL, Saucedo R (2011) The 17 July 1999 block-and-ash flow (BAF) at Colima Volcano: new insights on volcanic granular flows from textural analysis Journal of Volcanology and Geothermal Research 204:40-56 doi:https://doi.org/10.1016/j.jvolgeores.2011.04.013
Sbrana A, Cioni R, Marianelli P, Sulpizio R, Andronico D, Pasquini G (2020) Volcanic evolution of the Somma-Vesuvius Complex (Italy) Journal of Maps:1-11 doi:https://doi.org/10.1080/17445647.2019.1706653
Scarpati C, Sparice D, Perrotta A (2014) A crystal concentration method for calculating ignimbrite volume from distal ash-fall deposits and a reappraisal of the magnitude of the Campanian Ignimbrite Journal of Volcanology and Geothermal Research 280:67-75 doi:https://doi.org/10.1016/j.jvolgeores.2014.05.009
Selva J, Marzocchi W, Papale P, Sandri L (2012) Operational eruption forecasting at high-risk volcanoes: the case of Campi Flegrei, Naples J Appl Volcan 1:5
Spiller ET, Bayarri MJ, Berger JO, Calder ES, Patra AK, Pitman EB, Wolpert RL (2014) Automating emulator construction for geophysical hazard maps SIAM/ASA Journal on Uncertainty Quantification 2:126-152 doi:https://doi.org/10.1137/120899285
Sulpizio R, Mele D, Dellino P, La Volpe L (2005) A complex, Subplinian-type eruption from low-viscosity, phonolitic to tephri-phonolitic magma: the AD 472 (Pollena) eruption of Somma-Vesuvius, Italy Bulletin of volcanology 67:743-767 doi:https://doi.org/10.1007/s00445-005-0414-x
Sulpizio R, Mele D, Dellino P, La Volpe L (2007) Deposits and physical properties of pyroclastic density currents during complex Subplinian eruptions: the AD 472 (Pollena) eruption of Somma-Vesuvius, Italy Sedimentology 54:607–635 doi:10.1111/j.1365-3091.2006.00852.x

Sulpizio R, Dellino P (2008) Sedimentology, depositional mechanisms and pulsating behaviour of pyroclastic density currents Dev Volc 10:57-96
Tadini A, Bevilacqua A, Neri A, Cioni R, Aspinall WP, Bisson M, Isaia R, Mazzarini F, Valentine GAV, Vitale S, Baxter PJ, Bertagnini A, Cerminara M, de' Michieli Vitturi M, Di Roberto A, Engwell SL, Esposti Ongaro T, Flandoli F, Pistolesi M (2017a) Assessing future vent opening locations at the Somma-Vesuvio volcanic complex: 2. Probability maps of the caldera for a future Plinian/sub-Plinian event with uncertainty quantification Journal of Geophysical Research: Solid Earth 122:4357-4376 doi:10.1002/2016JB013860
Tadini A, Bisson M, Neri A, Cioni R, Bevilacqua A, Aspinall WP (2017b) Assessing future vent opening locations at the Somma-Vesuvio volcanic complex: 1. A new information geo-database with uncertainty characterizations Journal of Geophysical Research: Solid Earth 122:4336-4356 doi:10.1002/2016JB013858
Tierz P, Sandri L, Costa A, Zaccarelli L, Di Vito MA, Sulpizio R, Marzocchi W (2016) Suitability of energy cone for probabilistic volcanic hazard assessment: validation tests at Somma-Vesuvius and Campi Flegrei (Italy) Bulletin of Volcanology 78:79 doi:https://doi.org/10.1007/s00445-016-1073-9
Tierz P, Stefanescu ER, Sandri L, Sulpizio R, Valentine GA, Marzocchi W, Patra AK (2018) Towards Quantitative Volcanic Risk of Pyroclastic Density Currents: Probabilistic Hazard Curves and Maps Around Somma- Vesuvius (Italy) Journal of Geophysical Research: Solid Earth 123:6299-6317
Valentine GA, Palladino DM, DiemKaye K, Fletcher C (2019) Lithic-rich and lithic-poor ignimbrites and their basal deposits: Sovana and Sorano formations (Latera caldera, Italy) Bulletin of Volcanology 81:29 doi:https://doi.org/10.1007/s00445-019-1288-7
Valentine GA (2020) Initiation of dilute and concentrated pyroclastic currents from collapsing mixtures and origin of their proximal deposits Bulletin of Volcanology 82:20 doi:https://doi.org/10.1007/s00445-020-1366-x
Walker GPL (1980) The Taupo Pumice: product of the most powerful known (Ultraplinian) eruption? Journal of Volcanology and Geothermal Research 8:69-94 doi:https://doi.org/10.1016/0377-0273(80)90008-6
Walker GPL (1983) Ignimbrite types and ignimbrite problems Journal of volcanology and geothermal research 17:65-88 doi:https://doi.org/10.1016/0377-0273(83)90062-8
Wohletz KH, Sheridan MF, Brown WK (1989) Particle size distributions and the sequential fragmentation/transport theory applied to volcanic ash J Geophys Res-Sol Ea 94:15703-15721

FIGURE CAPTIONS

Figure 1 Landsat image of the Somma-Vesuvius area highlighting the localities cited in the text (courtesy U.S. Geological Survey, Department of the Interior). Coordinates are expressed in the UTM WGS84 33N cartographic system.

Figure 2 a) the EU3pf unit; b) the EU4 unit (with levels a, b and c); c) the F_g unit.

Figure 3 stratigraphic sections used to calculate the parameters of the EU3pf, EU4 and F_g (Cupa Olivella and Cupa Fontana lobes) units. Vent positions, vent uncertainty areas and Somma-Vesuvius caldera outline as defined in Tadini et al. (2017b).

Figure 4 example of the identification of two segments (Segment 1 in light orange and Segment 2 in dark orange) for the MRL_{50} of the EU4b unit. Starting from these two segments (and from the others that compose the whole outline), different uncertainty bounds are traced according to the amount and quality of the constraints available (inclined topography, proximity and thickness of stratigraphic sections, isopach lines).

Figure 5 a) MRL outlines and isopachs related to the EU3pf unit. The green dashed line identifies the north and south sectors used for volume and TGSD calculations; b) MRL outlines and isopachs related to the EU4b unit. The dark green

dashed line identifies the NW and SE sectors used for volume and TGSD calculations; c) MRL outlines related to the F_g Cupa Fontana and Cupa Olivella lobes. Preserved PDC deposits related to the AD 472 eruption (Santacroce and Sbrana 2003) are also shown. Vent positions, vent uncertainty areas and Somma-Vesuvius caldera outline as defined in Tadini et al. (2017b).

Figure 6 MRL outlines for the EU3pf and EU4b units and for the F_g Cupa Olivella and Cupa Fontana lobes as a function of the angle (in degree) from the North (in clockwise direction).

Figure 7 stratigraphic sections with samples and related Voronoi polygons used to calculate the TGSD of the: a) EU3pf unit. The green dashed line identifies the north and south sectors used for TGSD calculations; b) EU4b unit. The dark green dashed line identifies the NW and SE sectors used for TGSD calculations; c) EU4c unit; d) F_g (Cupa Olivella and Cupa Fontana lobes) unit. Vent positions, vent uncertainty areas and Somma-Vesuvius caldera outline as defined in Tadini et al. (2017b).

Figure 8 TGSD calculated by using the Voronoi tessellation method for the a) EU3pf (Total, North and South sectors), b) EU4b (Total, NW and SE sectors) and c) F_g (Cupa Olivella and Cupa Fontana lobes) units.

Figure 9 a) TGSD calculated for the EU4b unit by using the Voronoi tessellation method, the Isomass method with the formula of Pyle (1989) and the Isomass method with the Weibull function (Bonadonna and Houghton 2005); b) TGSD calculated for the EU4c unit by using the Voronoi tessellation method and the Isomass method with the formula of Pyle (1989); c) TGSD calculated for the EU4b/c unit (levels b and c considered together) by using the Voronoi tessellation method and the Isomass method with the formula of Pyle (1989).

TABLE CAPTIONS

Table 1 Maximum invaded areas (MIAs) for all the PDC units discussed. F_g CO and F_g CF are related to, respectively, to the Cupa Olivella and Cupa Fontana lobes.

Table 2 Methods used for volume estimation. Method names are: "CRh" – Crandell version 1; "CRs" – Crandell version 2; "TR" – trapezoid; "PY" – Pyle; "VOR" – voronoi; "TIN" – triangular irregular network.

Table 3 Slope classes, percentages of the MIA related to the MRL_{50} which belong to one of the three slope classes, number of stratigraphic sections which fall into one of the three slope classes and average thicknesses of the above-mentioned sections for all the units/lobes.

Table 4 volume estimations for the EU3pf unit using methods CRh, CRs, VOR and TIN.

Table 5 Volume estimations for the EU4 unit (level b) using method CRs, TR, PY, VOR and TIN.

870

871 **Table 6** Volume estimations for the “Cupa Fontana” and “Cupa Olivella” PDC lobes of the F_g unit using methods CRs,
872 (VOR) and TIN.

873

874 **Table 7** Summary of data used for TGSD estimations for all the studied units. The uncertainty on deposit density is related
875 to the standard deviation of the data.

Figure 1

Click here to access/download;Figure;Fig01.tif

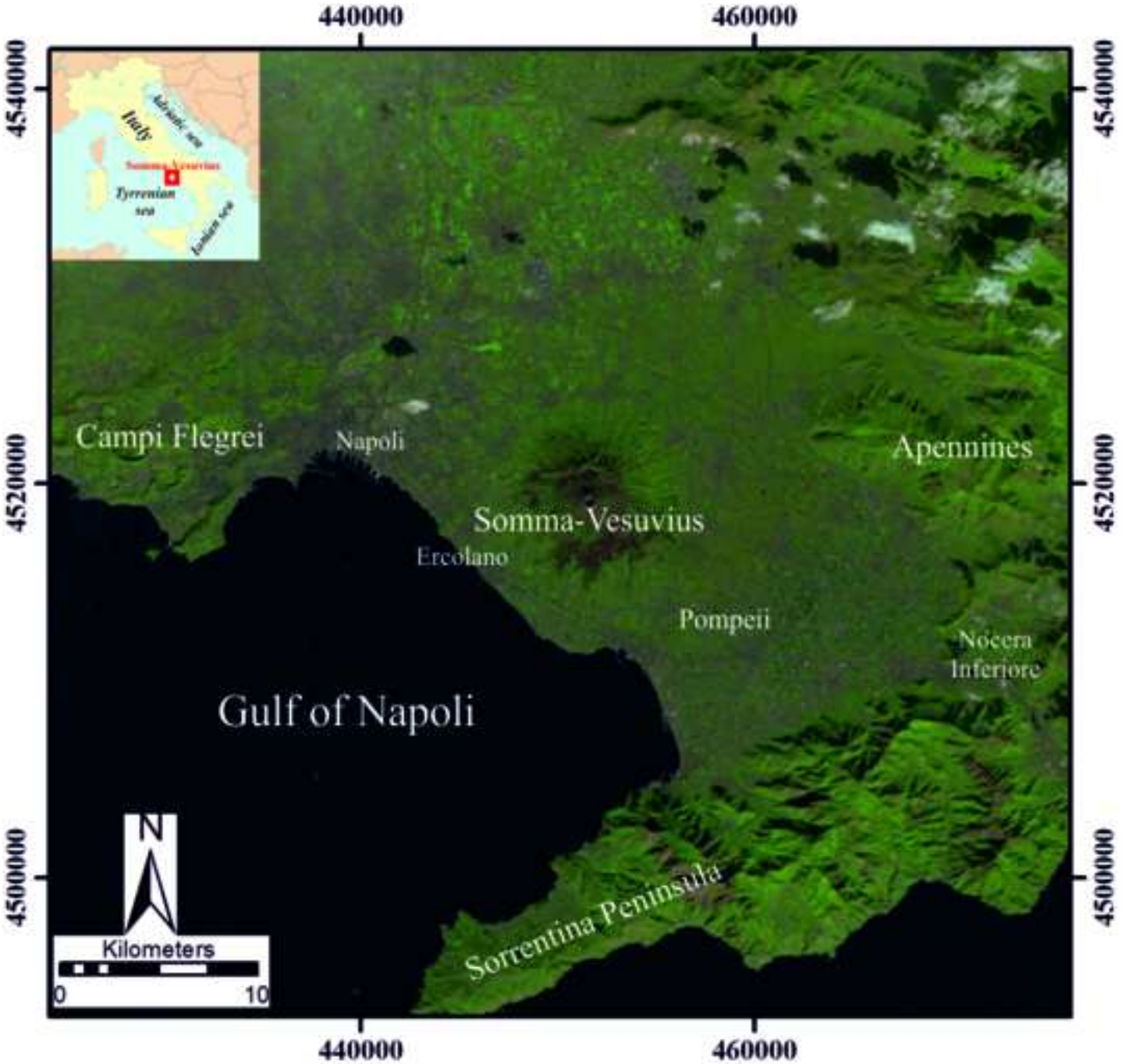

Figure 1 Landsat image of the Somma-Vesuvius area highlighting the localities cited in the text (courtesy U.S. Geological Survey, Department of the Interior). Coordinates are expressed in the UTM WGS84 33N cartographic system.

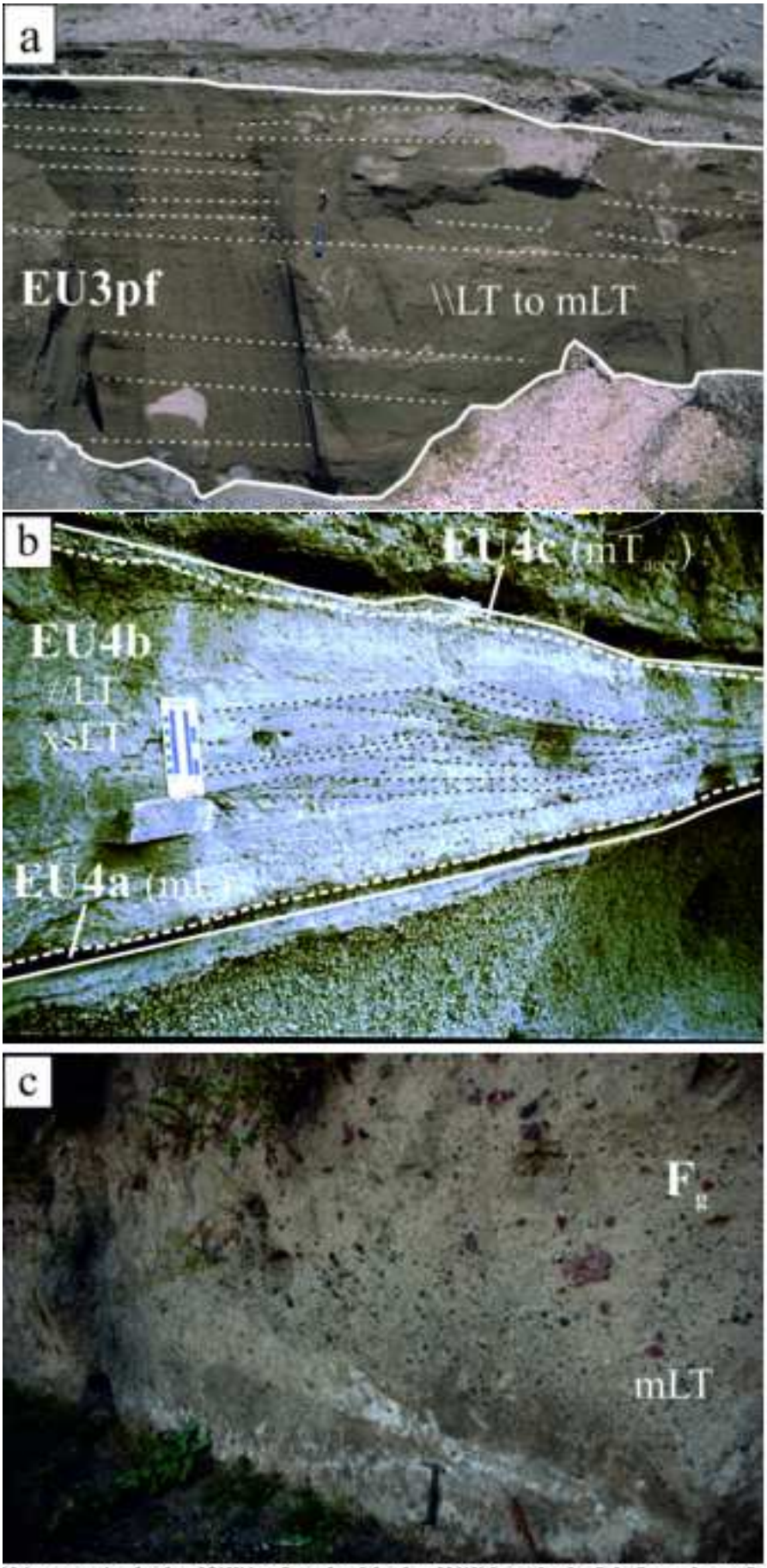

Figure 2 a) the EU3pf unit; b) the EU4 unit (with levels a, b and c); c) the F_g unit.

Figure 3

Click here to access/download;Figure;Fig03.tif

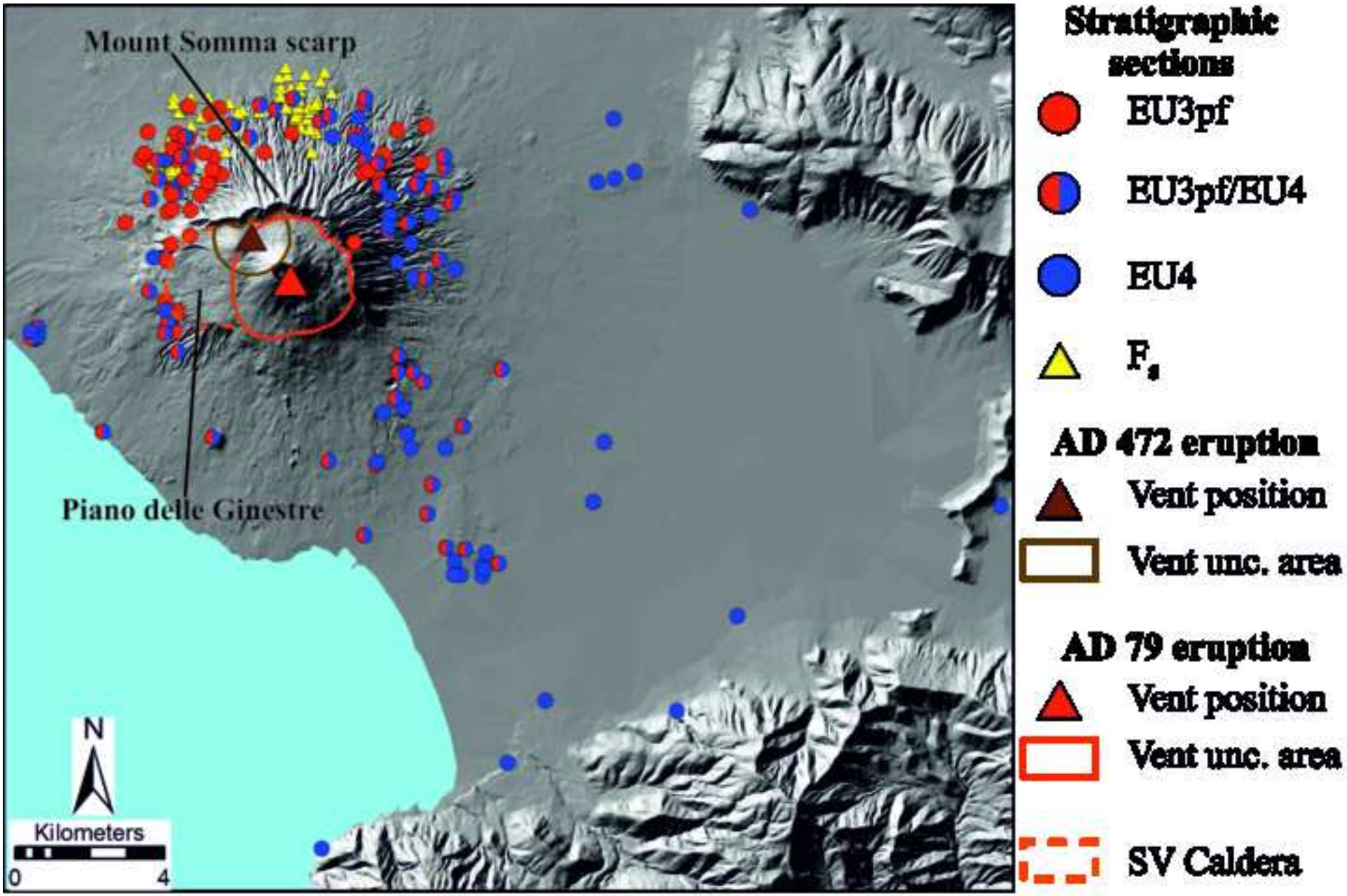

Figure 3 stratigraphic sections used to calculate the parameters of the EU3pf, EU4 and F_s (Cupa Olivelle and Cupa Fontana lobes) units. Vent positions, vent uncertainty areas and Somma-Vesuvius caldera outline as defined in Tadini et al. (2017b).

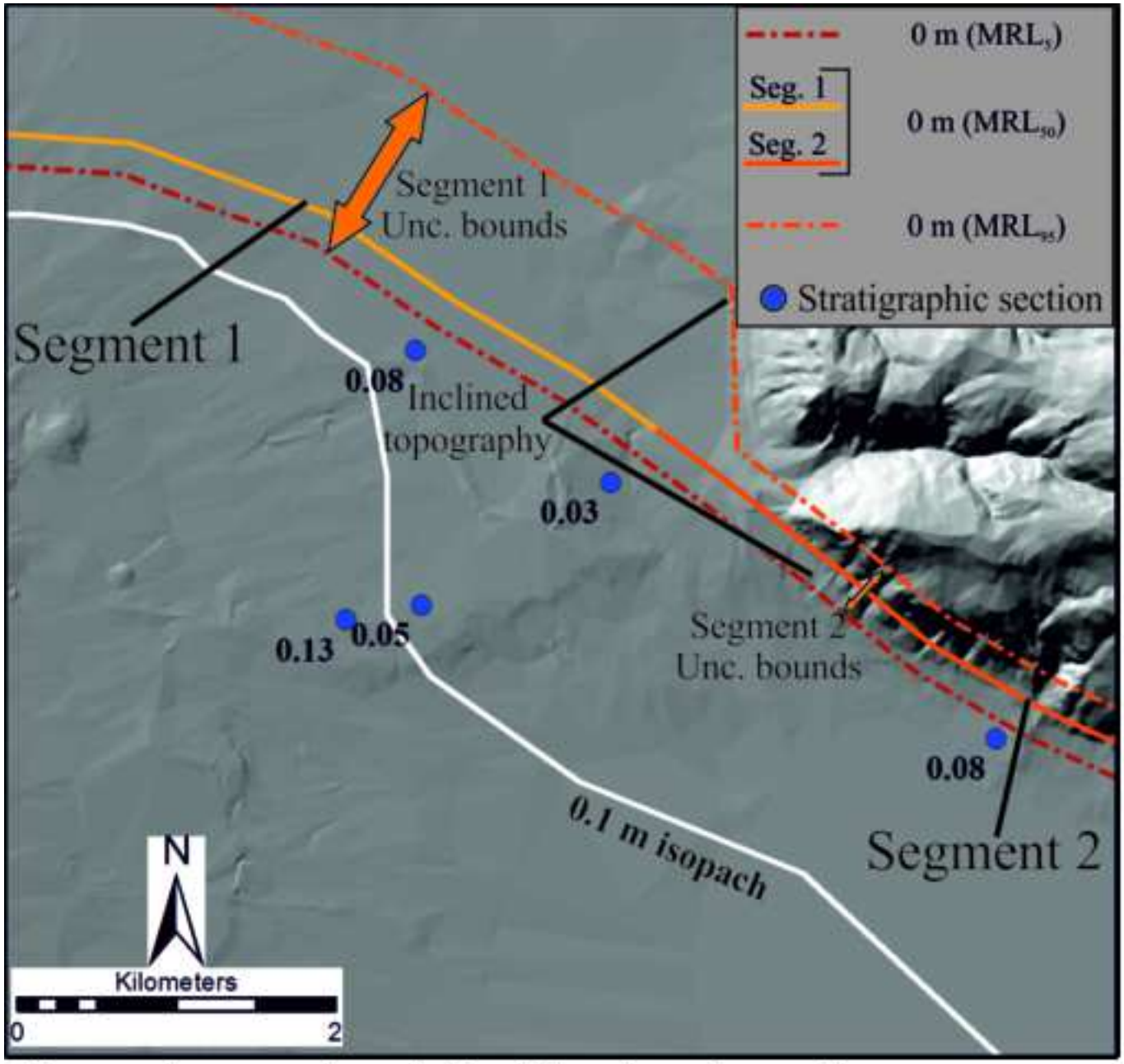

Figure 4 example of the identification of two segments (Segment 1 in light orange and Segment 2 in dark orange) for the MRL_{50} of the EU4b unit. Starting from these two segments (and from the others that compose the whole outline), different uncertainty bounds are traced according to the amount and quality of the constraints available (inclined topography, proximity and thickness of stratigraphic sections, isopach lines).

Figure 5

Click here to access/download;Figure;Fig05.tif

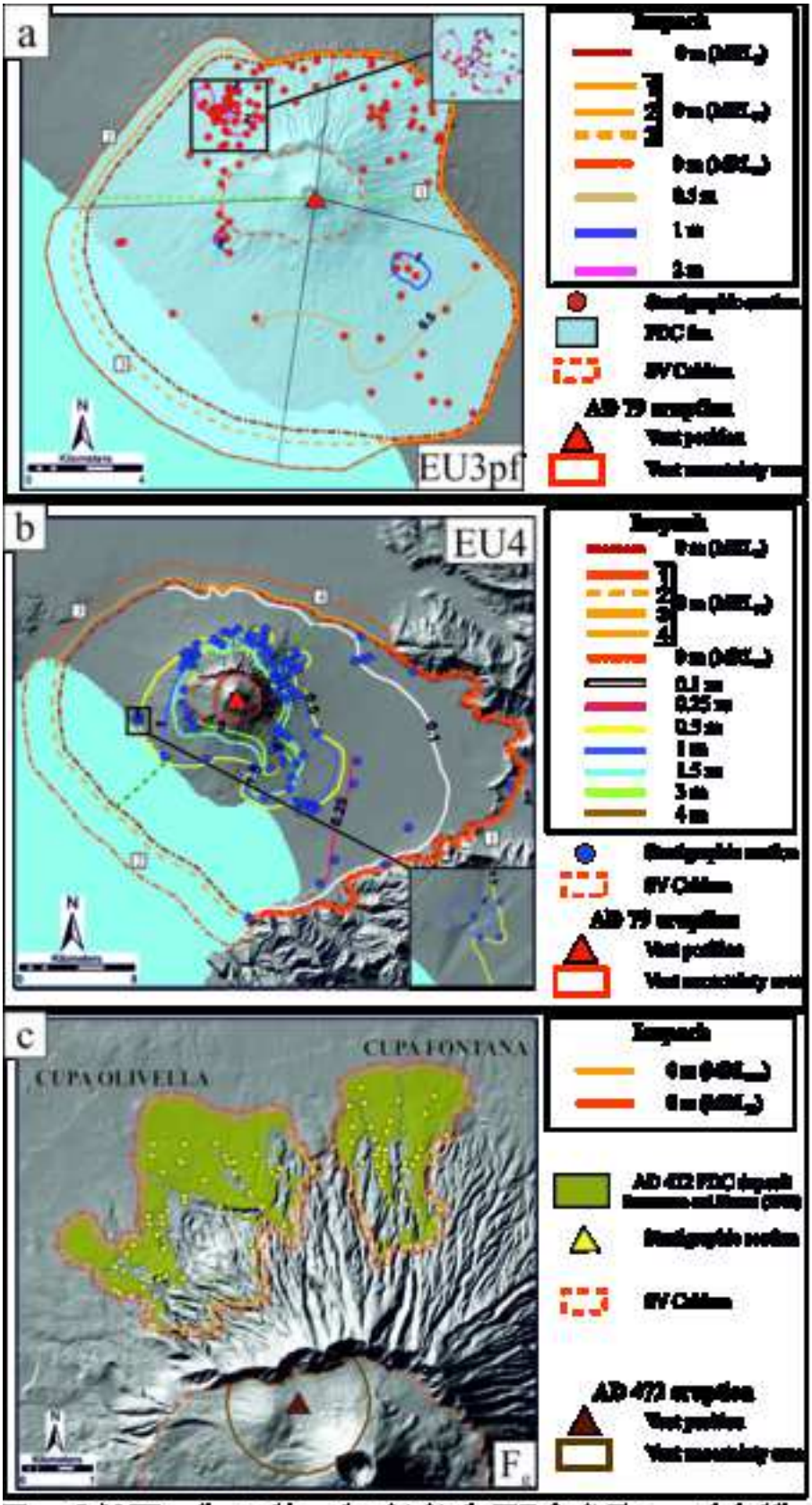

Figure 5 a) MEL-outlines and isopachs related to the EU3pf unit. The green dashed line identifies the north and south sectors used for volume and TGSD calculations; b) MEL-outlines and isopachs related to the EU4b unit. The dark green dashed line identifies the NW and SE sectors used for volume and TGSD calculations; c) MEL-outlines related to the F_c, Cupa Fontana and Cupa Olivella lobes. Preserved PDC deposits related to the AD 472 eruption (Santacroce and Sbrana 2003) are also shown. Vent positions, vent uncertainty areas and Somma-Vesuvius caldera outline as defined in Tadini et al. (2017b).

Figure 6

Click here to access/download;Figure;Fig06.tif

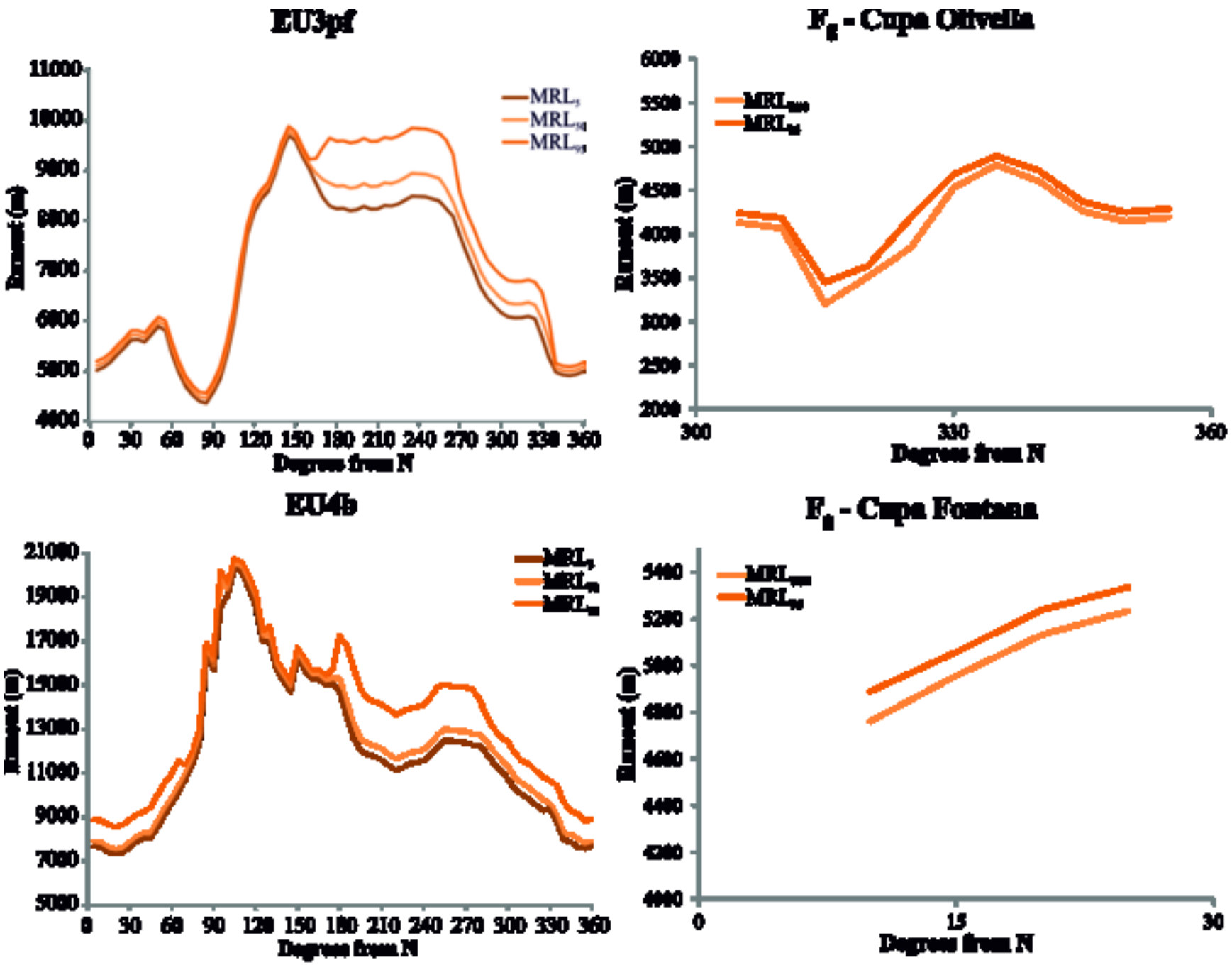

Figure 6 MRL outlines for the EU3pf and EU4b units and for the F_8 Cupa Olivella and Cupa Fontana lobes as a function of the angle (in degree) from the North (in clockwise direction).

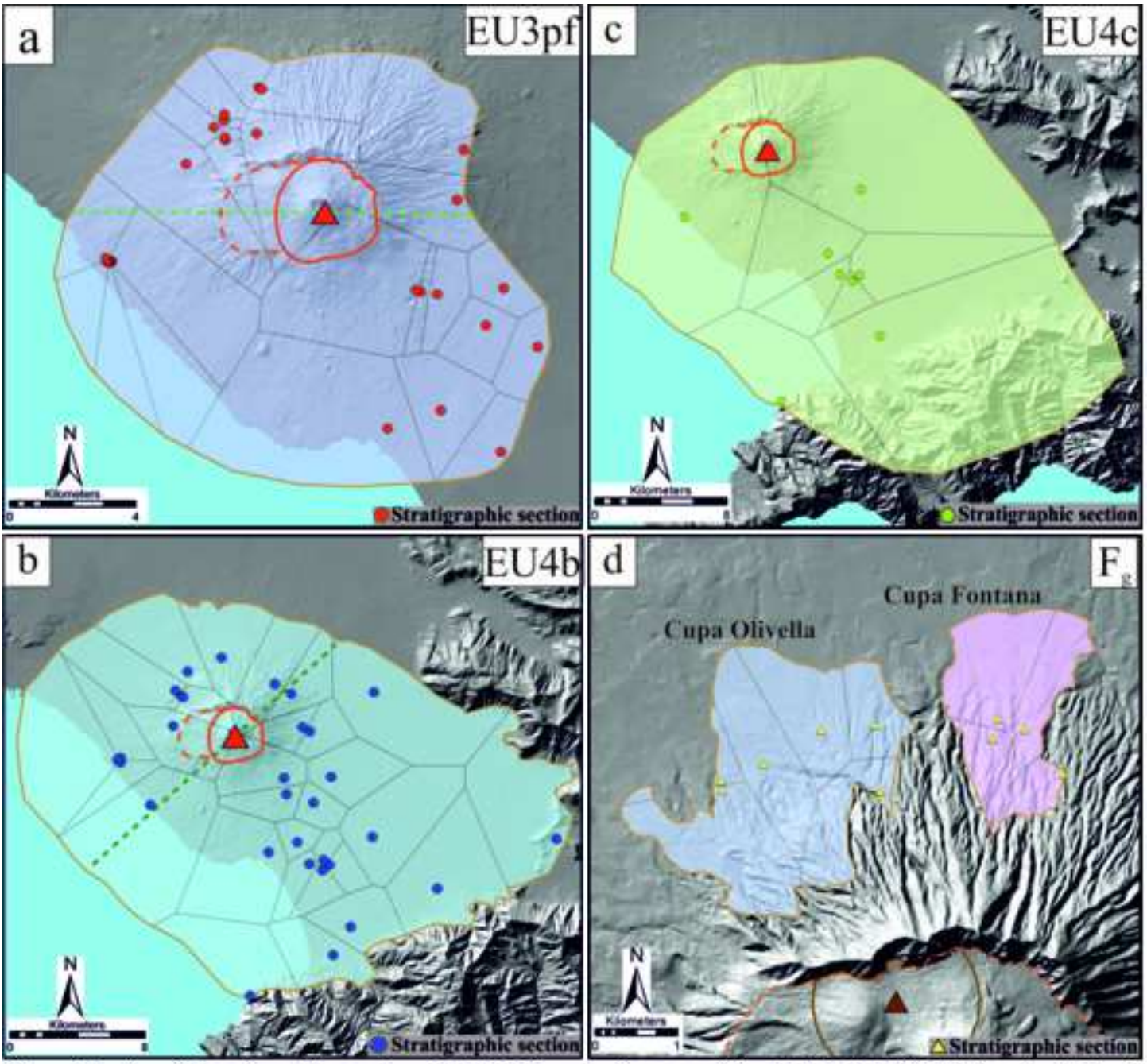

Figure 7 stratigraphic sections with samples and related Voronoi polygons used to calculate the TGSD of the: a) EU3pf unit. The green dashed line identifies the north and south sectors used for TGSD calculations; b) EU4b unit. The dark green dashed line identifies the NW and SE sectors used for TGSD calculations; c) EU4c unit; d) F_s (Cupa Olivella and Cupa Fontana lobes) unit. Vent positions, vent uncertainty areas and Somma-Vesuvius caldera outline as defined in Tadini et al. (2017b).

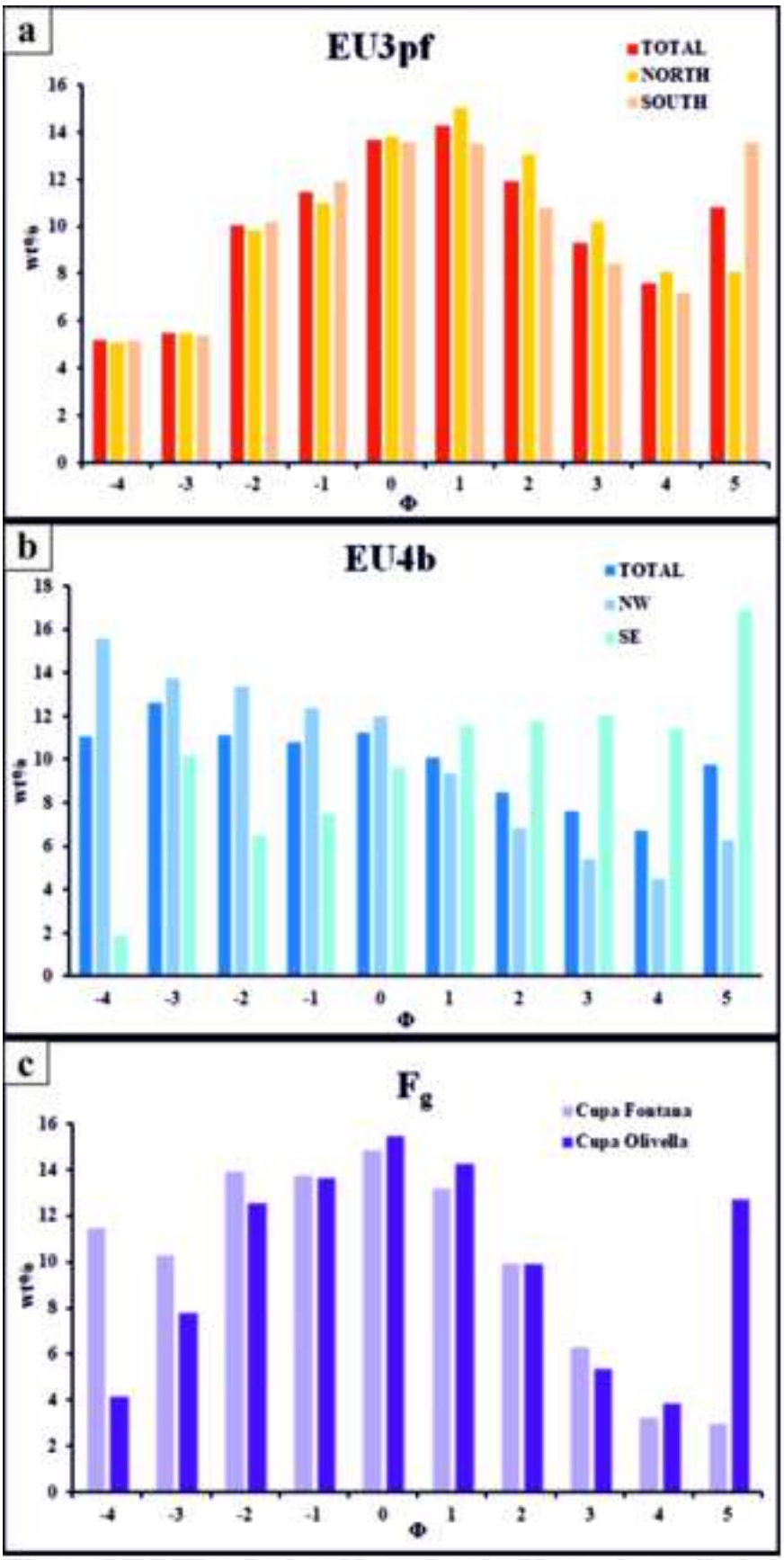

Figure 8 TGSD calculated by using the Voronoi tessellation method for the a) EU3pf (Total, North and South sectors), b) EU4b (Total, NW and SE sectors) and c) F_g (Cupa Olivella and Cupa Fontana lobes) units.

Figure 9

Click here to access/download;Figure;Fig09.tif

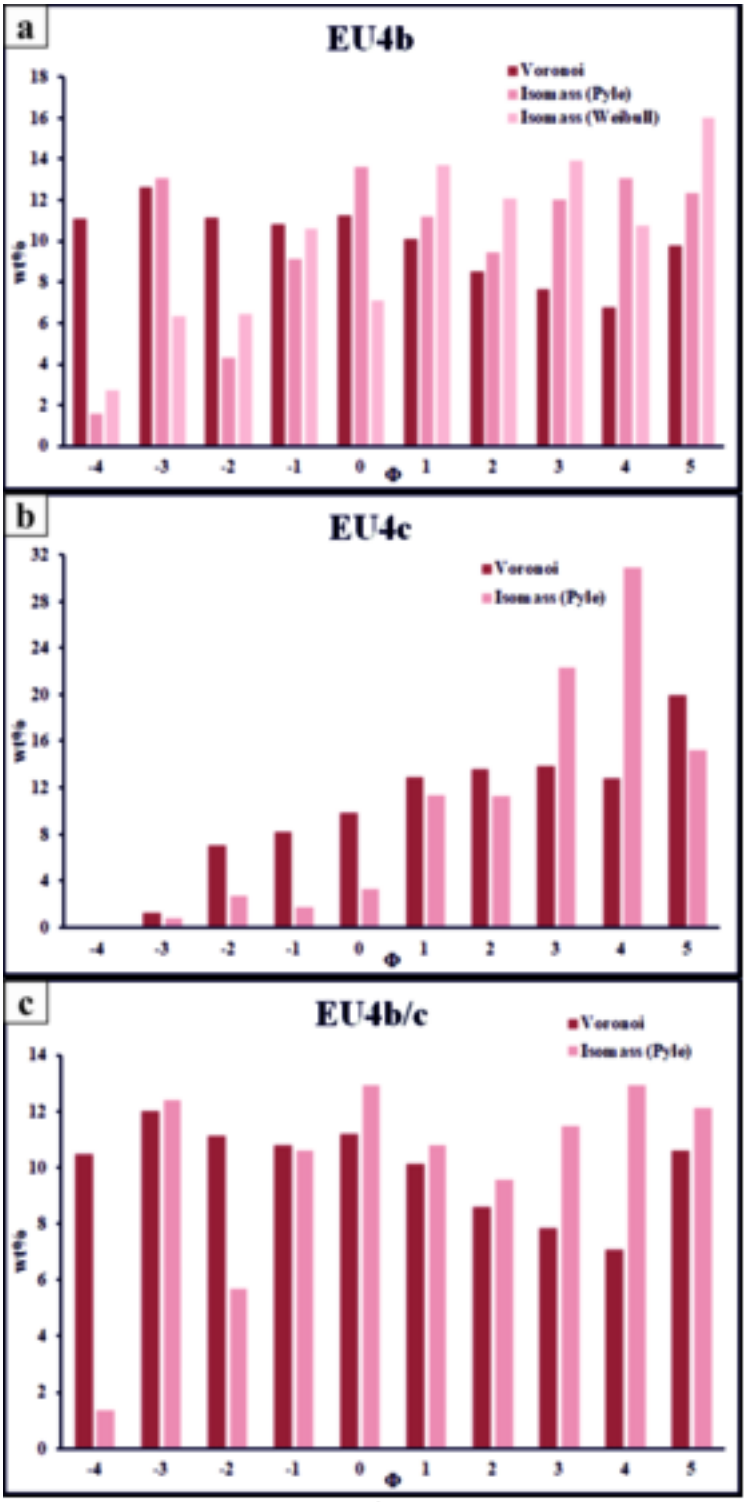

Figure 9 a) TGSD calculated for the EU4b unit by using the Voronoi tessellation method, the Isomass method with the formula of Pyle (1989) and the Isomass method with the Weibull function (Bernardova and Houghton 2005); b) TGSD calculated for the EU4c unit by using the Voronoi tessellation method and the Isomass method with the formula of Pyle (1989); c) TGSD calculated for the EU4b/c unit (levels b and c considered together) by using the Voronoi tessellation method and the Isomass method with the formula of Pyle (1989).

Table 1

UNIT	MIA (km^2)		
	5th	**50th**	**95th**
EU3pf	143	**166**	212
EU4b	492	**521**	610
F_g CO	-	**4.8**	5.7
F_g CF	-	**7.1**	8.1

Table 2

METHOD NAME	DESCRIPTION	UNITS FOR WHICH IT HAS BEEN USED	REFERENCE(S)
CRh	Partitioning of the deposit into homogeneous areas (PDC fans). Average value of thickness applied to the whole partition, whose volume is thickness*area. Total volume is the sum of the volumes of each partition.	EU3pf	Crandell (1989)
CRs	Similar to the above, but here defining areas or sectors in terms of topographic slopes, using the increments 0-15, 15-30, and >30 degrees.	EU3pf; EU4b; F_g	Crandell (1989)
TR	Dispersal area of the deposits is reported on isopach maps and each of them is plotted in a *thickness vs. area diagram* ; the resulting best fit curve is then integrated up to the 0-m thickness isopach.	EU4b	Fierstein and Nathenson (1992)
PY	Dispersal area of the deposits is reported on isopach maps and each of them plotted in a *ln thickness versus square root area diagram* ; the resulting best fit curve is then integrated up to the 0-m thickness isopach.	EU4b	Pyle (1989)
VOR	Partitioning (using a nearest-neighbor algorithm) of the study area in as many polygons as the number of stratigraphic sections, each polygon having the thickness measured in the corresponding data point. Total volume is the sum of the product of the area of each cell by its thickness. The 0-m thickness isopach used is the MRL_{50}.	EU3pf; EU4b; F_g	Voronoi (1908) Bonadonna and Houghton (2005)
TIN	Vector surface method that consists of a network of triangles formed by connecting nodes (measured thicknesses at vertexes) according to the Delaunay criterion. Thickness in each point of the triangles is calculated through linear interpolation between the data at their vertexes.	EU3pf; EU4b; F_g	Lee and Schachter (1980) Bisson and Del Carlo (2013)

Table 3

UNIT	SLOPE CLASSES (°)	% MIA 50th	N° SECTIONS	AVERAGE THICKNESS (m)
EU3pf	0-15	77	62	1.94
	15-30	16.2	33	1.63
	>30	6.8	11	1.37
EU4b	0-15	89.9	69	1.25
	15-30	7.2	31	1.2
	>30	2.9	2	1.39
F_g Cupa Olivella	0-15	67.9	24	4.11
	15-30	23.2	5	2.7
	>30	8.9	1	2
F_g Cupa Fontana	0-15	73.7	22	1.63
	15-30	21.8	5	1.7
	>30	4.5	-	-

Table 4

Method	Unit	Sector	MRL	Volume (km^3)
CRh	EU3pf	Total	MRL_{50}	**0.265**
CRs	EU3pf	Total	MRL_{50}	**0.267**
	EU4b			**0.507**
	Fg CF			**0.0053**
	Fg CO			**0.0234**
TR	EU4b	Total	MRL_{50}	**0.364**
PY	EU4b	Total	MRL_{50}	**0.334**
VOR	EU3pf	Total	MRL_{50}	**0.281**
	EU4b			**0.560**
	Fg CF			**0.0034**
	Fg CO			**0.0215**
TIN	EU3pf	North	MRL_5	0.089
			MRL_{50}	**0.096**
			MRL_{95}	0.100
		South	MRL_5	0.086
			MRL_{50}	**0.092**
			MRL_{95}	0.111
		Total	MRL_5	0.175
			MRL_{50}	**0.188**
			MRL_{95}	0.211
	EU4b	NW	MRL_5	0.119
			MRL_{50}	**0.12**
			MRL_{95}	0.133
		SE	MRL_5	0.175
			MRL_{50}	**0.175**
			MRL_{95}	0.179
		Total	MRL_5	0.292
			MRL_{50}	**0.295**
			MRL_{95}	0.313
	EU4c	Total	-	0.034
	Fg CF	Total	$MRL_{5/50}$	**0.0026**
			MRL_{95}	0.0029
	Fg CO	Total	$MRL_{5/50}$	**0.0121**
			MRL_{95}	0.0142

Table 5

Unit	Method(s) used for TGSD	Stratigraphic sections considered for TGSD	Samples used for TGSD	Samples used for deposit density
EU3pf	Voronoi	27	98	17
EU4b	Voronoi Isomass	31	68	18
EU4c	Voronoi Isomass	8	8	2
F_g Cupa Fontana	Voronoi	4	4	18
F_g Cupa Olivella	Voronoi	6	6	2

Deposit density (kg/m^3)
1120 ± 250
1308 ± 171
1336 ± 85
1676 ± 96
1195 ± 97

Online Resource 1

Click here to access/download

Supplementary Material

ESM_1.xlsx

Online Resource 2

Click here to access/download

Supplementary Material

ESM_2.pdf

Online Resource 3

Click here to access/download

Supplementary Material

ESM_3.pdf

Online Resource 4

Click here to access/download

Supplementary Material

ESM_4.pdf

Click here to access/download
Supplementary Material
ESM_captions.pdf